การคงอยู่ของความผันผวนของความสูงในแบบจำลองโมเลกุลาร์บีมเอพิแทกซี

นายพิพิธธน แสนสีหา

PERSISTENCE OF HEIGHT FLUCTUATION IN MOLECULAR-BEAM

EPITAXY MODEL

Mr. Pipitton Sanseeha
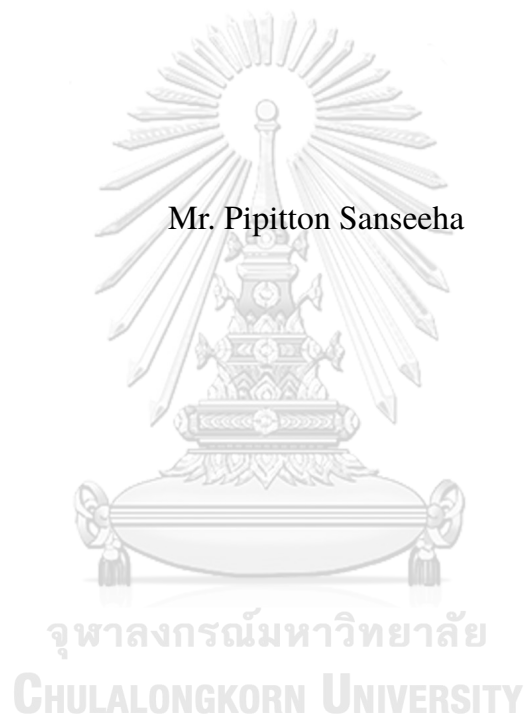
A Thesis Submitted in Partial Fulfillment of the Requirements

for the Degree of Master of Science Program in Physics

Department of Physics

Faculty of Science

Chulalongkorn University

Academic Year 2022

Thesis Title	PERSISTENCE OF HEIGHT FLUCTUATION IN MOLECULAR-BEAM EPITAXY MODEL
By	Mr. Pipitton Sanseeha
Field of Study	Physics
Thesis Advisor	Assistant Professor Rangsima Chanphana, Ph.D.
Thesis Co-Advisor	Assistant Professor Patcha Chatraphorn, Ph.D.

Accepted by the Faculty of Science, Chulalongkorn University in Partial Fulfillment of the Requirements for the Master's Degree

.... Dean of the Faculty of Science

(Professor Polkit Sangvanich, Ph.D.)

THESIS COMMITTEE

.... Chairman

(Assistant Professor Paisan Tooprakai, Ph.D.)

.... Thesis Advisor

(Assistant Professor Rangsima Chanphana, Ph.D.)

.... Thesis Co-advisor

(Assistant Professor Patcha Chatraphorn, Ph.D.)

.... Examiner

(Assistant Professor Noravee Kanchanavatee , Ph.D.)

.... External Examiner

(Assistant Professor Manit Klawtanong, Ph.D.)

พิพิธธน แสนสีหา: การคงอยู่ของความผันผวนของความสูงในแบบจำลองโมเลกุลาร์บีมเอพิแทกซี. (PERSISTENCE OF HEIGHT FLUCTUATION IN MOLECULAR-BEAM EPITAXY MODEL) อ.ที่ปรึกษาวิทยานิพนธ์หลัก : ผศ. ดร. รังสิมา ชาญพนา, อ.ที่ปรึกษาวิทยานิพนธ์ร่วม : ผศ. ดร. ปัจฉา ฉัตราภรณ์ 51 หน้า.

ความน่าจะเป็นของการคงอยู่เป็นปริมาณที่น่าสนใจในกระบวนการสโตแคสติกซึ่งเป็นพลวัตในงานประเภทปลูกผิวของเรา ความน่าจะเป็นของการคงอยู่ของความผันผวนของความสูงคือความน่าจะเป็นที่ค่าความผันผวนของความสูงไม่กลับสู่ค่าเริ่มต้นตลอดช่วงเวลาหนึ่ง ในการศึกษาครั้งนี้ เราทำการศึกษาความน่าจะเป็นของการคงอยู่ของแบบจำลองโมเลกุลาร์บีมเอพิแทกซี (MBE model) ซึ่งเป็นแบบจำลองการปลูกฟิล์มแบบโมเลกุลาร์บีมเอพิแทกซีด้วยวิธีทางตัวเลข ในครึ่งแรก เราศึกษาผลของอัตราการปลูกฟิล์มและอุณหภูมิต่อเลขชี้กำลังการเติบโต (β) และเลขชี้กำลังการคงอยู่ (θ) สำหรับอุณหภูมิที่ทำให้อะตอมที่ผิวหน้ามีระยะทางการแพร่เท่ากับ 1 หน่วย เราได้เลขชี้กำลังของการเติบโตประมาณ 0.17 และเลขชี้กำลังการคงอยู่ประมาณ 0.78 เมื่ออุณหภูมิเพิ่มขึ้นเลขชี้กำลังการเติบโตจะลดลงในขณะที่เลขชี้กำลังการคงอยู่เพิ่มขึ้น ผลที่ได้นี้เกิดขึ้นเช่นเดียวกันเมื่อเราลดอัตราการปลูกฟิล์ม ในส่วนที่สอง เราศึกษาความน่าจะเป็นของการคงอยู่ที่เปลี่ยนไปเมื่อเราทำการพิจารณาค่าความผันผวนของความสูงเริ่มต้นเฉพาะค่า ความน่าจะเป็นของการคงอยู่ด้านลบของความผันผวนของความสูงค่าบวกลดลงตามเวลาแบบกฎการยกกำลังก็ต่อเมื่อพิจารณาค่าของความผันผวนของความสูงเริ่มต้นที่มากกว่าค่าความกว้างของอินเตอร์เฟซอิ่มตัว ความน่าจะเป็นของการคงอยู่ด้านบวกของความผันผวนของความสูงค่าลบไม่ลดลงตามเวลาแบบกฎการยกกำลัง จนกระทั่งเมื่อพิจารณาค่าของความผันผวนของความสูงเริ่มต้นที่มากกว่าค่าความกว้างของอินเตอร์เฟซอิ่มตัวมากๆ เราวัดความน่าจะเป็นของการคงอยู่สำหรับค่าความผันผวนของความสูงเริ่มต้น,ขนาดของระบบ, และช่วงเวลาตัวอย่างเพื่อหาความสัมพันธ์ของมาตราส่วน ความน่าจะเป็นของการคงอยู่เป็นฟังก์ชัน 3 พารามิเตอร์, $f(\frac{t}{L^z}, \frac{\delta t}{L^z}, \frac{|h_0|}{L^\alpha})$

ภาควิชา	ฟิสิกส์	ลายมือชื่อนิสิต	....
สาขาวิชา	ฟิสิกส์	ลายมือชื่อ อ.ที่ปรึกษาหลัก	....
ปีการศึกษา	2565	ลายมือชื่อ อ.ที่ปรึกษาร่วม	....

6270078423: MAJOR PHYSICS
KEYWORDS: PERSISTENCE PROBABILITY / MOLECULAR-BEAM EPI-TAXY / MBE

PIPITTON SANSEEHA : PERSISTENCE OF HEIGHT FLUCTUATION IN MOLECULAR-BEAM EPITAXY MODEL. ADVISOR : Asst. Prof. Dr. Rangsima Chanphana, THESIS COADVISOR : Asst. Prof. Dr. Patcha Cha-traphorn, 51 pp.

Persistence probability is an interesting quantity in stochastic process which is the dynamics of surface growth in this study. Persistence probability of height fluctuation is the probability that the height fluctuation does not return to its initial value throughout a time interval. In this work, we use a numerical simulation approach to investigate the persistence probability in Molecular-Beam Epitaxy (MBE) model which is associated with Molecular-Beam Epitaxy technique. First half, we study the effects of temperature and deposition rate on the growth exponent (β) and persistence exponent (θ). For the temperature corresponds to 1 diffusion length, we get $\beta \approx 0.17$ and positive steady-state persistence exponent, $\theta_+^S \approx 0.78$. When the temperature increases, the growth exponent value decreases while the persistence exponent rises. The same results happen when the deposition rate is decreased. On the second half, we investigate how the persistence probabilities change with a particular initial value of height fluctuation. The negative persistence probability of positive initial height shows power law when the initial height is slightly greater than w_{sat}. The positive persistence probability of negative initial height does not show power law decay unless the initial height is much greater than w_{sat}. We measure the relationship of persistence probability on initial height fluctuation (h_0), system size, and discrete sampling time to investigate the scaling relation. The persistence probability is a function of three parameters, $f(\frac{t}{L^z}, \frac{\delta t}{L^z}, \frac{|h_0|}{L^\alpha})$.

Department:	Physics	Student's Signature	....
Field of Study:	Physics	Advisor's Signature	....
Academic Year:	2022	Co-advisor's Signature	....

Acknowledgements

CONTENTS

LIST OF TABLES

LIST OF FIGURES

Chapter I

INTRODUCTION

Persistence probability has been extensively researched in the random process problems (Aurzada and Simon, 2015; Samia and Lutscher, 2012; Sire et al., 2000; Williams and Araéjo, 2000; Aurzada and Kilian, 2022). The applications of persistence concept are diverse, including those in financial (Ren and Zheng, 2003) and microbiological system (Şimşek and Kim, 2019). This concept is also involved in physics such as Burger's equation which is convection-diffusion in fluid mechanics (She et al., 1992), wetting model (Efraim and Taitelbaum, 2011), Ising model (Majumdar et al., 1996) and interface fluctuations (Majumdar and Bray, 2001). Previous studies of persistence probability show fascinating results for both physics and statistics. This quantity can describe the nature of random processes and predict the dynamical evolution of any random variable.

Persistence probabilities in surface growth have received considerably interest recently (Chanphana and Chatraphorn, 2019a,b; Chanphana et al., 2013; Constantin et al., 2004b; Dougherty et al., 2002; Krug et al., 1997) because their properties are found to be related to one of the critical exponents at an early time of thin-film growth. We can examine how atoms develop with time. Persistence probabilities of averaged and specific values of height fluctuation also show fractal behavior and scale invariance property. According to Krug and coworkers (Krug et al., 1997), the persistence probability of height fluctuation $P(t)$ is the probability that the height fluctuation h does not return to its initial value h_0 throughout a certain time interval. When the height fluctuation continues to be larger than its initial value, the persistence probability is categorized as the positive persistence probability (P_+). On the other hand, when the height fluctuation remains smaller than its initial value, the probability is classified as the negative persistence probability (P_-). Both positive and negative persistence probabilities show power law decay with time. The probabilities scales with time (t) as $P_\pm(t) \propto t^{-\theta_\pm}$ where θ_+ and θ_- are the positive and negative persistence exponents, respectively (Krug et al., 1997). The unit of t in this work is monolayer (ML). This means that the time it takes for the film to grow one complete atomic layer is 1 ML. In the steady-state when the film roughness stops increasing, the persistence probability is called steady-state persistence probability $P^S(t)$ and the obtained exponent is called steady-state persistence exponent θ^S. θ^S is found to relate to the growth exponent β of the model (Krug et al., 1997; Constantin et al., 2004b).

Previous results of the persistence probability of height fluctuation are obtained from atomistic "toy" models, such as the Family (Family, 1986) and Das Sarma Tamborenea (DT) models (Das Sarma and Tamborenea, 1991; Tamborenea and Das Sarma, 1993). Their diffusion rules consist of random deposition and sim-

ple surface diffusion processes, but do not directly involve atomic type and effects of the surface temperature, deposition rate, and bonding energy which are known to govern the film morphology (Guan et al., 2019; Marconi et al., 2016; Tabe et al., 1981). In this work, we study the molecular-beam epitaxy (MBE) model, a more realistic model which reflects the actual thin film growth technique. Experimental parameters such as the growth temperature and deposition rate are adjustable in this model. Film morphology and statistical quantities are investigated after temperatures and deposition rates are varied.

The MBE technique is a thin film growth technique that deposits atoms on a substrate through vaporization. An element source was heated in effusion cells then the element is evaporated through ultra-high vacuum chamber and deposited on the substrate (Franchi, 2013). The atom deposition rate can be controlled via the cell shutter. This allows us to grow a pure film in layer-by-layer mode (Franchi, 2013; Morresi, 2013). A thin film that is grown by the MBE technique has the same orientation with its substrate. This technique is best known for semiconductor manufacturing (Hotta et al., 2022; Rangel-Kuoppa et al., 2021). With the ability to grow very precise and very thin films (with thickness in the order of nanometers), the nanostructures can be made by this technique (Koguchi et al., 1991; Sadowski et al., 2007). Because of this experimental advantage, many simulations and modelling studies of MBE process have been pursued (Barnett and Rockett, 1988; Fornari et al., 2018; Kazantsev et al., 2015; Liang et al., 2020) in order to obtain more understanding of the process and to be able to better control the process. The simulated thin films also possess interesting statistical properties (Léonard et al., 1997; Luis et al., 2019). Additionally, the film morphology and dynamic scaling exponents of the MBE model at relatively low temperature are similar to those of the DT model with single surface diffusion length (Chanphana, 2013).

The first goal of this work is to investigate how the growth and persistence exponents vary with growth parameters which are temperature and deposition rate. Another objective is to observe the persistence exponent when only a particular initial height fluctuation is taken into account and to determine the scaling behavior of the persistence probability.

This thesis is organized as follow. Chapter 1 contains an introduction. The molecular-beam epitaxy model is described in chapter 2. In chapter 3, the persistence probability and its scaling relation are addressed. We examine effects of temperature and deposition rate on the growth exponent (β) and persistence exponent (θ) in chapter 4. In this chapter, we show film morphologies of thin film grown in different temperature. The relation between θ^S_+, θ^S_- and β is summarized. Effects of h_0 on the persistence probabilities, the scaling behavior of $P^S_\pm(t, L, \delta t, |h_0|)$ are also included in this chapter. Lastly, the conclusion is in chapter 5.

Chapter II

MOLECULAR-BEAM EPITAXY MODEL

In this chapter, we introduce the Molecular-beam epitaxy model for thin film growth. In this model, the molecular-beam epitaxy technique is simulated using three processes i.e., the deposition, desorption and diffusion processes. All parameters that influence the atomic diffusion along the surface are described. The calculation of the diffusion time and the surface diffusion length is included in this chapter.

2.1   The Molecular-beam epitaxy model and processes

The Molecular-beam epitaxy (MBE) model is used in this work to simulate the thin film growing technique under ultra-high vacuum (UHV) environment. Molecular beam evaporated from Knudsen effusion cells (K-cells) is deposited on a heated substrate (Franchi, 2013; Holloway and McGuire, 2008). The MBE technique is helpful to custom the controls to perform a thin layer of 1 atomic thickness (Morresi, 2013). There are 2 controlling parameters that we are interested in i.e., the growth temperature of the substrate and the deposition rate. These parameters play important role in the roughness of the film surface (Barabási and Stanley, 1995).

To simulate a discrete model of MBE, we study its microscopic processes of growing thin film (Arthur Jr, 1968; Barabási and Stanley, 1995; Das Sarma, 1996; Das Sarma and Tamborenea, 1991; Franchi, 2013; Holloway and McGuire, 2008; Morresi, 2013). The simulation steps in the model are designed to mimic the three main MBE processes: deposition, desorption, and diffusion. Details of each process are explained below.

1. Deposition process

Atoms are randomly deposited on the substrate with an equal probability on each site. When only the deposition process is taken into account, the MBE model is similar to the random deposition (RD) model (Barabási and Stanley, 1995). The rule of the RD model is that atoms are deposited randomly with no correlation with any previously deposited atom.

We introduce a basic concept of deposition in $(d + 1)$-dimensional system

where atoms fall on to a surface in d dimension and grow in the direction that is perpendicular to the surface. The deposition rate (F) indicates how fast we let atoms fall on our substrates. It is usually measured as number of monolayer (ML) that can be grown in a unit time, thus unit of the deposition rate is ML/s. In a system with one dimensional substrate of a size L, the deposition rate of F ML/s means that ($F \times L$) atoms are deposited on the substrate in the time period of one second. Another quantity considered is the deposition time (t_F) of an atom, which is simply $(F \times L)^{-1}$ in one dimensional substrate. In other words, the deposition time is the amount of time between two deposited atoms. In ($d + 1$)-dimensional system, the deposition time is generalized to be

$$t_F = (F \times L^d)^{-1}. \tag{2.1}$$

2. Desorption process

The deposited atom can be desorbed from the substrate surface if it can form only weak bonds to the surface atoms. The desorption probability of an atom depends on its characteristic desorption energy (E_D) and substrate temperature (T). The desorption time (τ_D) is expressed by the Arrhenius law (Arthur Jr, 1968; Barabási and Stanley, 1995):

$$\tau_D = \phi_0 \, exp(\frac{E_D}{k_B T}). \tag{2.2}$$

where $\phi_0 \approx 10^{-14}, E_D \approx 2.4$ eV (for Ga on GaAs (111) substrate (Arthur Jr, 1968)) and k_B is Boltzmann constant. Barabási & Stanley (Barabási and Stanley, 1995) has shown that at low to intermediate temperature, for example, $T \leq 750$ K for Ga on GaAs (111) substrate, the desorption can be negligible, by the reason that the desorption time is much larger than the deposition time. For higher temperature, desorption process will play more important role. In this research, very high temperature is not considered. The surface atom has a chance to desorb from the surface but with much less probability compared to the other two processes, so desorption is neglected.

3. Diffusion process

After an atom is deposited, it can hop to one of the nearest neighboring sites or a further site depending on the substrate temperature and its binding energy. The number of hops per unit time is expressed by the Arrhenius law (Barabási and Stanley, 1995; Kellogg et al., 1978):

$$N = \omega_D \, exp(-\frac{E_0 + nE_b}{k_B T}), \tag{2.3}$$

where N is the hopping rate of any atom, ω_D is the Debye frequency, E_0 is the activation energy, n is the number of bonds, E_b is the energy per bond and T is the

n	Diffusion time, τ_R, (s)				
	$T = 700$ K	$T = 725$ K	$T = 750$ K	$T = 775$ K	$T = 800$ K
1	7.85e-3	3.60e-5	1.74e-5	8.80e-6	4.64e-6
2	1.13e-2	4.39e-3	1.81e-3	7.86e-4	3.60e-4
3	1.64e0	5.34e-1	1.87e-1	7.02e-2	2.80e-2
4	2.37e+2	6.50e+1	1.94e+1	6.27e0	2.17e0
5	3.42e+4	7.91e+3	2.01e+3	5.60e+2	1.68e+2

Table 2.1: Diffusion time for Si atoms.

substrate temperature (Barabási and Stanley, 1995). For an atom that sticks to its neighbors, it requires the energy $E = E_0 + nE_b$ to break its bonds in order to diffuse. But if the atom has no lateral bond, it needs only the energy $E = E_0$ to overcome the lattice potential.

From the Arrhenius law, the diffusion time, τ_R, which is the time that an atom takes to diffuse to one of its nearest neighbors, is a function of E_0, n, E_b and T as

$$\tau_R = \tau_0 \, exp(\frac{E_0 + nE_B}{k_B T}), \tag{2.4}$$

where $\tau_0 = \frac{h}{2k_B T}$, is the inverse frequency of atomic vibration in crystal (Kittel, 2010). In our work, we try to simulate a simple MBE model. Silicon is chosen as both the substrate and the deposited atoms. In this work, we choose $E_0 = 1$ eV and $E_b = 0.3$ eV which are values of the Si (100) surface (Smith et al., 1995). Table 2.1 shows the calculated diffusion times for an Si atom deposited on Si (100) with n bonds at various substrate temperatures.
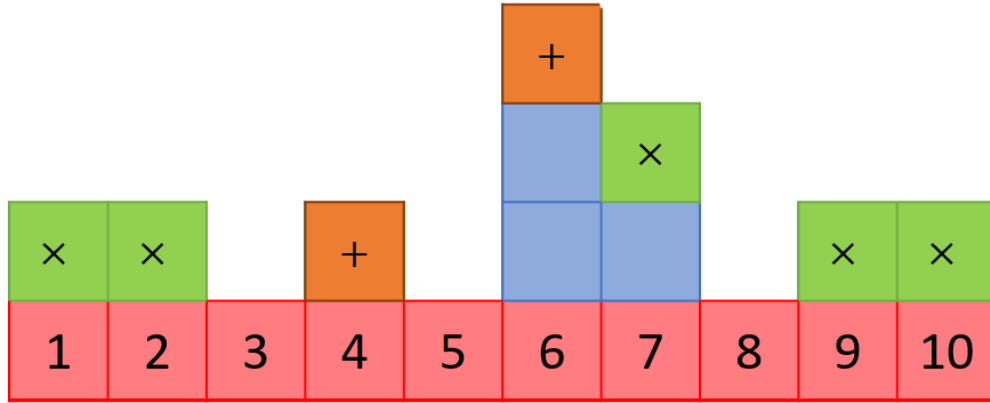
Figure 2.1: Diagram of the (1+1) MBE model.

Numbers in Table 2.1 show that the diffusion time decreases when we increase the substrate temperature, this shows that atoms can hop more easily with high hopping rate as the substrate temperature rises. At the same temperature, the diffusion time increases by about 100 times for every additional bond.

For simplicity of understanding, we present a diagram of the MBE model in one dimensional substrate with 10 atomic sizes in Figure 2.1. The substrate atoms are 1-10 red boxes. At both ends of the substrate, we assign periodic boundary conditions i.e. if an atom at site 1 is hopping to the left, the atom will land on site 10. The surface atoms are the top atom in each column, which are those green boxes with "×" and orange boxes with "+" in the diagram. From the configuration in this diagram, when we calculate the hopping probability of all surface atoms, only orange with "+" atoms can hop because their hopping rate is about 100 times higher than others. For two dimensional substrates, bonding numbers are computed as shown in Figure 2.2.

Figure 2.2 illustrates how to compute the number of bonds by counting the number of sides the deposited atom touches. Figure 2.2 (a) shows that after deposition, the yellow atom has 1 bond with the atom below. If the diffusion time is less than the deposition time, it can diffuse to any nearest neighboring site. The yellow atom in Figure 2.2 (b) forms 3 bonds with neighbors and substrate and can diffuse to any direction if it has enough energy to break the bonds and with the condition $\tau_R < \tau_F$.

τ_F in equation (2.1) tells us the time required before a new atom is deposited, whereas τ_R in equation (2.4) represents the time it takes for a deposited atom to hop. Between each deposition, all surface atoms with $\tau_R < \tau_F$ can diffuse to one of the nearest sites. The atom with lower τ_R has higher probability of hopping. The
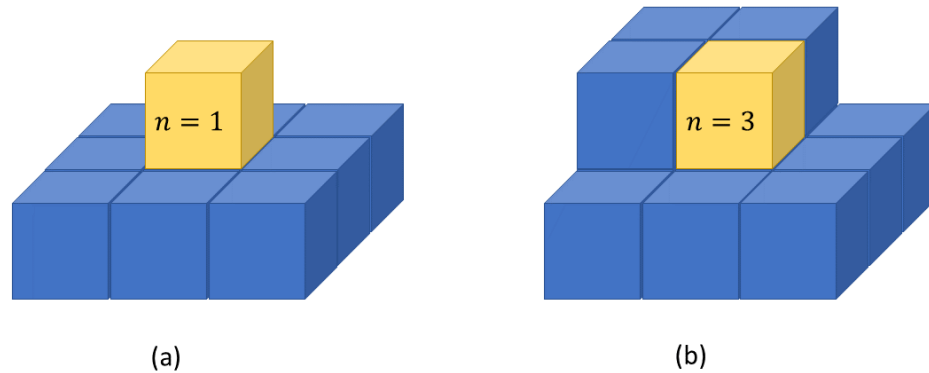
Figure 2.2: The number of bonds (n) of the deposited atom (a) $n = 1$, (b) $n = 3$.

number of hopping steps that an atom can hop is called the diffusion length (l), which can be calculated from the ratio τ_F/τ_R as expressed in equation (2.5).

$$l = \frac{1}{(F \times L^d)} / (\tau_0 \, exp(\frac{E_0 + nE_B}{k_B T})).$$

(2.5)

According to equation (2.5), increasing the substrate temperature lengthens the surface diffusion length. In contrast, increasing the deposition rate results in a reduction in the diffusion length.

More details on how the diffusion length varies with temperature and deposition rates are reported in chapter 4.

2.2 Interface width and critical exponents of MBE model

The interface width (w) is a quantity that describes roughness of the interface. It is defined as the root mean square fluctuation in the height, H, (Barabási and
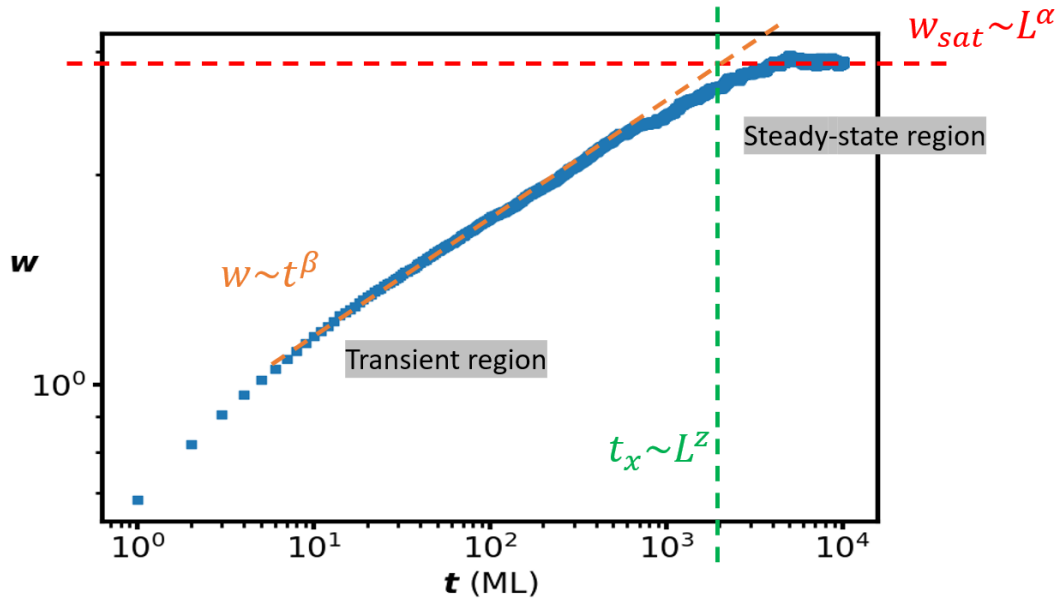
Figure 2.3: Interface width for the MBE model of the system size $L \times L = 50 \times 50$ sites.

Stanley, 1995).

$$w(L,t) = \sqrt{\frac{1}{L^d} \sum_{i=1}^{L^d} [H(i,t) - \bar{H}(t)]^2}, \qquad (2.6)$$

where H is the height of each site on the substrate and $\bar{H}(t)$ is the mean height at time t. w is actually the standard deviation of the height of the grown films. So, this is a quantity that describe the roughness of the film surfaces.

The plots of interface width versus time in the log-log scale are shown in figure 2.3. There are 2 separated regimes. In the first regime, w evolves with time. This is called "transient region". Figure 2.3 shows that the interface width grows as a power of time, $w(L,t) \sim t^\beta$, β is the growth exponent. The second region takes place when the value of w stops increasing and becomes constant. It is called "saturated region" or the steady-state region. The saturation width, w_{sat}, increases as a power of the system size, L, as $w_{sat}(L,t) \sim L^\alpha$, where α is the roughness exponent. So, when we plot w vs t, we will observe large crossover time for large L. The time that w vs t curve changes from transient to steady-state is "cross-over time (t_x)". t_x is found to scale with L^z, where z is the dynamical exponent. The interface width is observed to be self-affine fractal which has scale invariance (Barabási and Stanley, 1995). Information extracted from the w vs t plot can determine the critical exponents (α, β, z) that characterize the universality class of the model used to simulate the film. For models with the same set of critical exponents, we can say that they are in the same "universality class" (Barabási and Stanley, 1995). They share the same dynamics scaling behavior.

In this dissertation we obtain critical exponents of the MBE model by using the data collapse method. We follow Family-Vicsek scaling relation (Family and Vicsek, 1985) to determine α, β and z. Step 1, we obtain $w(t)$ for different system sizes as shown in figure 2.4. Step 2, we rescale $w(L, t)$ with L^α and rescale t by L^z with varying values of the two exponents until all plots collapse on the same curve. The set of exponents when the plots are collapsed as shown in figure 2.5 is the set of critical exponents of the model being explored.
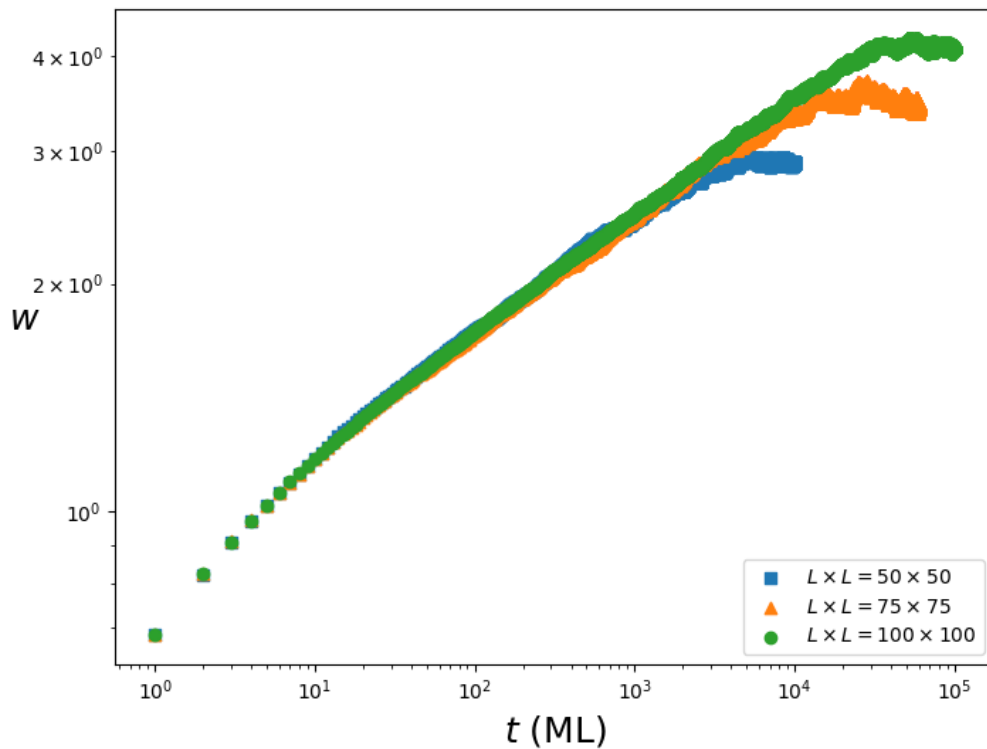

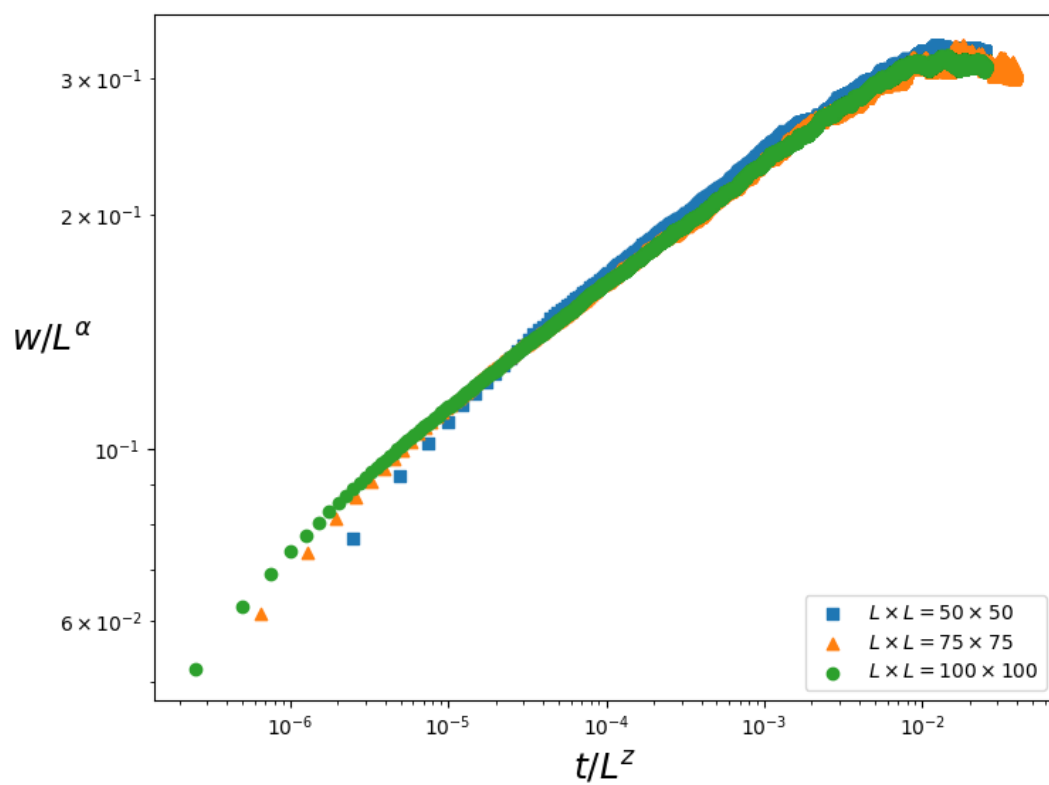Figure 2.4: The interface width of MBE model with three different system sizes.

Figure 2.5: Scaling plots showing the data collapse of the MBE model.

Figure 2.4 shows the plots of w vs t of the (2+1)-MBE model with $l = 1$ for three different system sizes i.e., $L \times L = 50 \times 50$, 75×75 and 100×100 sites. It is clearly seen that the film interface takes longer time to saturate and w_{sat} is higher for bigger system sizes. w_{sat} are observed to obey the relation $w_{sat}(L) \sim L^{\alpha}$. In figure 2.5, we rescale $w(L,t)$ with L^{α} and vary α until all plots saturate at the same value. For horizontal axis, we rescale t with L^{z} with varying z to shift all plots to have the same crossover time. After adjusting α and z until all plots approximately collapse into a single curve, β is calculated from the slope in the transient stage where $w(t) \sim t^{\beta}$. The best set of α, β and z forms the set of critical exponents for our model. So, from our simulation results, we found that $\alpha \approx 0.56$, $\beta \approx 0.17$ and $z \approx 3.30$ are the best set for collapsing our data of the (2+1)-MBE model with $l = 1$ and these values are consistent with the Family-Vicsek scaling relation (Family and Vicsek, 1985): $\frac{\alpha}{\beta} \approx z$.

In theory, the non-linear continuum growth equation that describes the MBE equation (Barabási and Stanley, 1995; Lai and Das Sarma, 1991) is:

$$\frac{\partial H(x,t)}{\partial t} = -K\nabla^4 H + \lambda_1 \nabla^2 (\nabla H)^2 + F + \eta, \qquad (2.7)$$

where $H(x,t)$ is interface height at position x and time t. F is flux of particles arriving at site x. K and λ_1 are constants. η is the uncorrelated random noise in which the average is zero and the second moment is $2D\delta^d(x - x')\delta(t - t')$, where d is system dimensions and D is diffusion coefficient. The $K\nabla^4 H$ and non-linear $\lambda_1 \nabla^2 (\nabla H)^2$ terms are described surface diffusion. The non-linear term in equation (2.7) makes up-down symmetry ($H \rightarrow -H$) absent for the MBE model.

From equation (2.7), the scaling exponents of the (2+1)-dimensional MBE model are obtained to be $\alpha = 0.67$, $\beta = 0.20$ and $z = 3.30$ (Barabási and Stanley, 1995) which all satisfy the relation $\frac{\alpha}{\beta} \approx z$. However, according to our simulation, the critical exponents are slightly lower than those from the MBE equation. The non-linear MBE equation describes thin film growth in continuum limit where the system size goes to infinity, this is the reason why the exponents are a bit different from our results.

Chapter III

PERSISTENCE PROBABILITY OF

HEIGHT-FLUCTUATION

In this chapter, we describe the transient and steady-state persistence probabilities. We discuss two categories of probabilities, their exponents, and the relationship between θ and β. We present that the non-linear term in the MBE equation causes the inequality of the persistence exponents. Results of the persistence probabilities as a function of the initial height fluctuation are shown. Lastly, the scaling behavior of the persistence probability is studied.
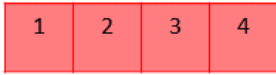
3.1   Persistence probability

From the perspective of nature, the persistence probability ($P(t)$) measures a quantity's memory. It tells us how long the value will remain unchanged. For the study of dynamical fluctuations in height profile of thin film growth, $P(t)$ is the probability that the $h(t)$ does not cross h_0 over a certain period of time. The height fluctuation of site i at time t, $h(i,t)$, is defined as $h(i,t) = H(i,t) - \bar{H}(t)$, where $H(i,t)$ is the height of site i at time t and $\bar{H}(t)$ is the average height at the same time.

A detailed example of how we calculate the persistence probability of average height fluctuation are shown in figure 3.1. For this example, we consider a flat substrate with 4 atomic sites and exclude random deposition and diffusion processes. Step 1, we start measuring the persistence probability at $t = 0$ ML when no atom has been deposited. At this time $\bar{H} = 0$ and the initial height fluctuations of each site are $h_0 = [0, 0, 0, 0]$ as shown in figure 3.1 (a). Step 2, we deposit 4 atoms (which equals the number of atoms in the substrate), the time becomes 1 ML and the average height is $\bar{H} = 1$ represented by the red dash line in figure 3.1 (b). Because we deposit 2 atoms on the first site and another 2 atoms on the third site in this illustration, the height fluctuations of each site at $t = 1$ ML are $h = [1, -1, 1, -1]$. At sites 1 and 3, h are greater than h_0, so we collect these sites for $P_+(t)$ type. For sites 2 and 4, $h < h_0$, thus we collect these sites for $P_-(t)$ type. At $t = 1$ ML, $P_+ = \frac{1}{2}$ and $P_- = \frac{1}{2}$. Step 3 shows configuration at $t = 2$ ML, another layer of atoms is deposited (3 atoms at site 2 and one at site 4) and $\bar{H} = 2$. h of sites 1 and 3 equal $h_0 = 0$, they violate condition to have nonzero of P_+, so at this time $P_+(t) = 0$. h of site 2, which is grouped in P_- type, is higher than its h_0, so the negative persistence probability of this site is zero. For site 4, we observe that $h < h_0$ which is consistent with the condition to have nonzero P_-, so we keep measuring P_- of this site. At $t = 2$ ML, $P_+ = 0$ and $P_- = \frac{1}{4}$.

$t = 0$ ML, $\overline{H}(0) = 0$
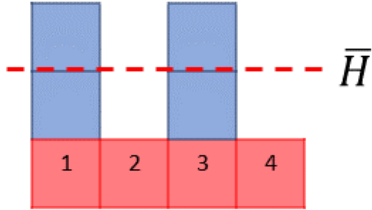$H(0) = [0,0,0,0]$
$h_0 = [0,0,0,0]$

(a)

$t = 1$ ML, $\overline{H}(1) = 1$
$H(1) = [2,0,2,0]$
$h(1) = [1,-1,1,-1]$
$h_0 = [0,0,0,0]$
$p = [+,-,+,-]$
$P_+ = 2/4$
$P_- = 2/4$

(b)

$t = 2$ ML, $\overline{H}(2) = 2$
$H(2) = [2,3,2,1]$
$h(2) = [0,1,0,-1]$
$h_0 = [0,0,0,0]$
$p = [0,0,0,-]$
$P_+ = 0$
$P_- = 1/4$

(c)
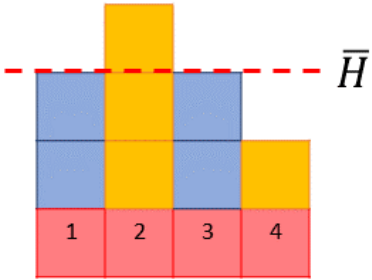
Figure 3.1: Schematic illustration of the persistence probability measurement process.
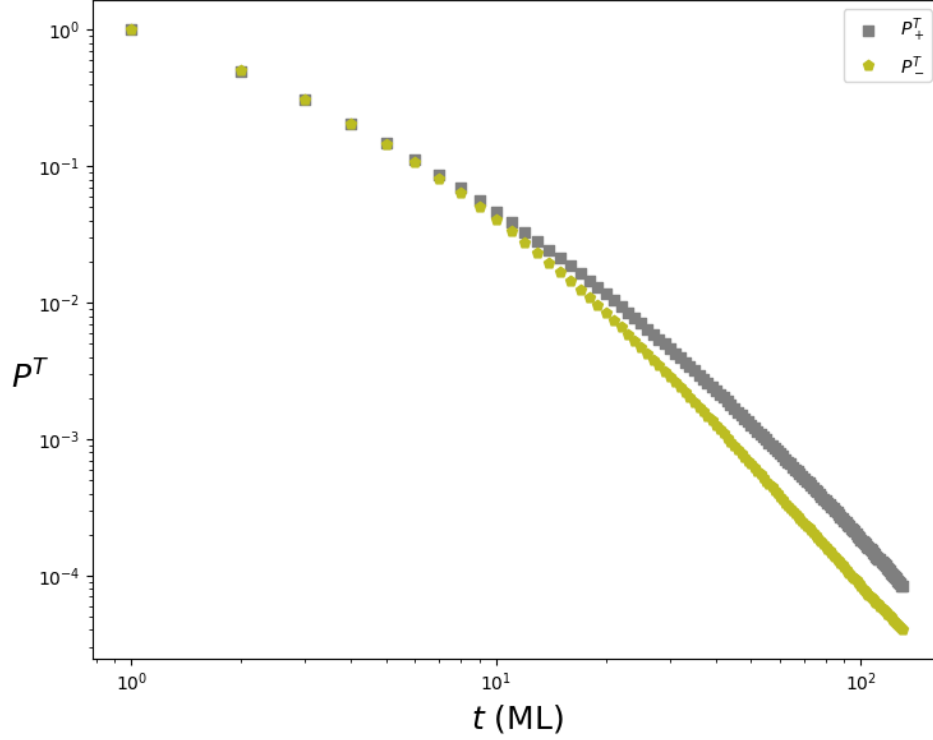
Figure 3.2: Transient persistence probability of the (2+1) MBE model. θ_+^T are not correlated with the dynamic scaling exponent.

According to Krug and coworkers (Krug et al., 1997), the persistence probability calculated by averaging over all initial heights exhibits power law decay with time. As the growth process is divided into 2 regions: transient and steady-state regions, $P(t)$ can also be calculated from 2 regions. The difference in them is the way the initial time (t_0), which is the time used to determine h_0, is chosen. For the transient persistence probabilities, the initial time is in the transient region, while the initial time must be in the steady-state region for the steady-state persistence probabilities. The transient persistence probabilities are observed to scale with the growth time as $P_\pm^T \propto t^{-\theta_\pm^T}$, while the steady-state persistence probabilities decay with time with the different rate as $P_\pm^S \propto t^{-\theta_\pm^S}$, where $\theta^T \neq \theta^S$ in general. In our simulations, $P_\pm^T$ are measured from an initial flat substrate, $h_0 = 0$ at $(t_0 = 0\,\mathrm{ML})$. For some models, $P_\pm^T$ plots do not clearly show a power-law decay. For instance, $P_\pm^T$ rapidly decrease to zero in the (2+1)-dimensional Family model (Constantin et al., 2004b), whose surface morphology is very smooth (Family, 1986). For the (2+1)-MBE model with $l_{max} = 1$, our simulated film surface is quite rough with deep grooves. $P_\pm^T$ show short range of the power-law decay during $t \sim 30 - 100$ ML as shown in figure 3.2. We obtain $\theta_+^T \approx 1.71$, $\theta_-^T \approx 1.43$.

For $P_\pm^S$, the initial time (t_0) depends on the saturation time of each model. $P_\pm^S$ plots decrease with time as a power-law in all growth models studied in the literatures (Chanphana et al., 2013; Chanphana and Chatraphorn, 2021; Krug et al.,
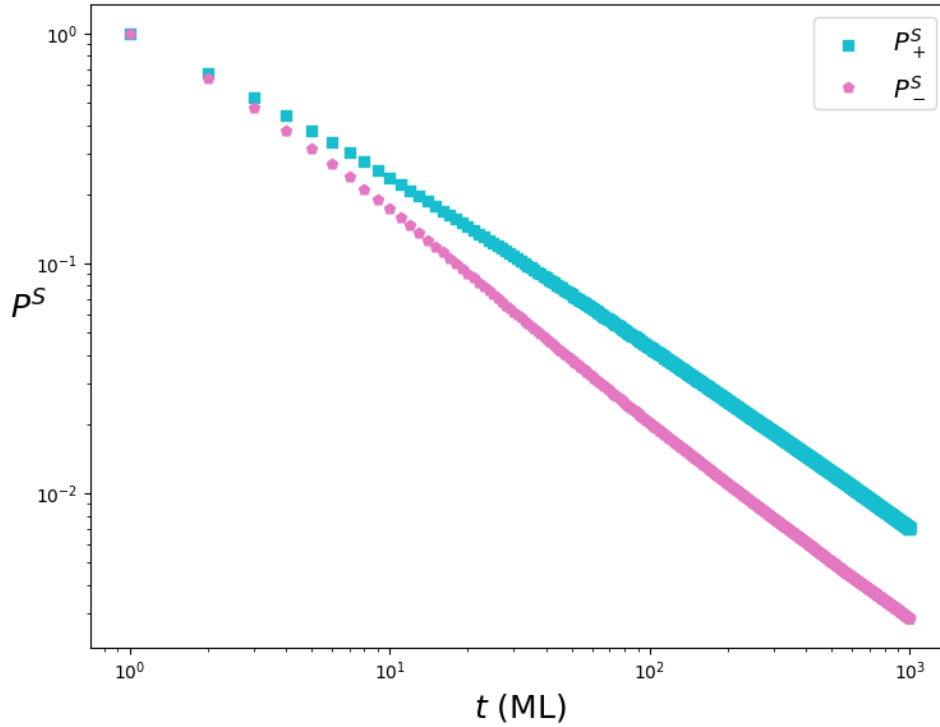
Figure 3.3: Steady-state persistence probability of the (2+1) MBE model.

1997). Figure 3.3 shows our $P^S_{\pm}$ versus time plots for the MBE model of $L \times L = 100 \times 100$ sites, $t_0 = 60,000$ ML. We obtain $\theta^S_+ \approx 0.78$ and $\theta^S_- \approx 0.90$ which are smaller than $\theta^T_{\pm}$.

Krug and coworkers (Krug et al., 1997) suggests that if the system can be described by linear Langevin equation, then steady-state persistence exponents relate the growth exponent β as

$$\theta^S_+ = \theta^S_- = 1 - \beta. \tag{3.1}$$

Constantin and coworkers (Constantin et al., 2004b) extends eq.3.1 to cover nonlinear growth processes as

$$\beta = max[1 - \theta^S_+, 1 - \theta^S_-]. \tag{3.2}$$

As can be seen from the figure 3.2 and 3.3, $\theta_+ \neq \theta_-$ for both regions. These inequalities show up-down asymmetric behavior which is generated from non-linear term (Ballestad et al., 2001; Barabási and Stanley, 1995) in eq. 2.7. In this work, we attempt to verify whether the relation in eq. 3.2 is valid in the MBE model.

Chanphana & Chatraphorn (Chanphana and Chatraphorn, 2019a) demonstrated that the diffusion length (l) affects the value of the persistence exponents. In our work, l can be varied by adjusting the growth parameters i.e., the substrate

temperature, and the deposition rate. Many studies suggest that increasing the deposition rate leads to the increase of the film roughness (Maboudian et al., 1994; Pal and Landau, 1994) which may affect the value of $\theta_\pm^T$ and $\theta_\pm^S$. In our study, effects of the growth temperature and the deposition rate on the persistence probabilities and exponents in the MBE model are investigated.

3.2   Scaling behavior of persistence probability

Previous works on persistence of interface fluctuations (Chanphana et al., 2013; Chanphana and Chatraphorn, 2019a, 2021; Constantin et al., 2004b; Krug et al., 1997; Dougherty et al., 2002) show that the steady-state persistence probability $P_\pm^S(t)$ of all initial height fluctuations exhibits power law decay with time as stated earlier. So, time is considered as one of the scaling variables. Constantin and coworkers (Constantin et al., 2004b) found that $P_\pm^S(t)$ exhibit power law when $t \ll L^z$. Decreasing system size causes the decrease in β, because the interface of small L becomes saturated more quickly due to the finite size effect (Krug and Meakin, 1990). Besides, $\theta_\pm^S$ increase when L is decreased. Another scaling variable is the size of the sampling time (δt) which is the discrete time interval between two measurements (Dougherty et al., 2005). The minimum value of (δt) is 1 ML. All the persistence probabilities from the previous chapter are measured at every monolayer, corresponding to $\delta t = 1$. As δt is increased, $P_\pm^S$ increase. This can be explained as follows. To calculate the persistence probability, number of sites whose h does not cross h_0 is counted while the sites whose h crosses h_0 are eliminated. If (δt) is large, it is possible that h of a certain site already crosses h_0 and then crosses back before we do the counting. In this situation, we count that site as "persisted" because we cannot detect the crossing of h, while the site would have been eliminated if δt is small enough for us to notice the crossing. This leads to large probabilities when δt is large. Effects of the sampling time have been widely studied in persistence probability probability (Constantin et al., 2004a; Dougherty et al., 2005) and other statistical quantities in stochastic process such as the survival probability (Chanphana and Chatraphorn, 2019b). Time scales of the growth process must depend on the cross-over time which is scaled with L^z. As a result, $P_\pm^S$ should scale with t/L^z and $\delta t/L^z$). The scaling behavior of $P_\pm^S(t, L, \delta t)$ is found to be $f_\pm(t/L^z, \delta t/L^z)$, where $t/L^z \ll 1$ and $\delta t/L^z \ll 1$ (Constantin et al., 2004b).

Effects of initial height fluctuation on $P_\pm^S$ of linear models was introduced by Chanphana and coworkers Chanphana et al. (2013) The persistence probabilities of a specific value of h_0 are denoted by $P_\pm^S(h_0, t)$. Figure 3.4 shows the example of how to choose sites with a desired h_0. The long rectangular unshaded block represents 100 completed layers already grown on a one dimensional substrate of 10 sites. The 10 blue boxes are the atoms in the 101st layer. At $t_0 = 101$ ML, if the persistence probability of $h_0 = 1$ is measured, only the sites 2, 3 and 8 (green boxes with an arrow pointing to them) are taken into account. At a later time, $t = t_0 + \delta t$, sites
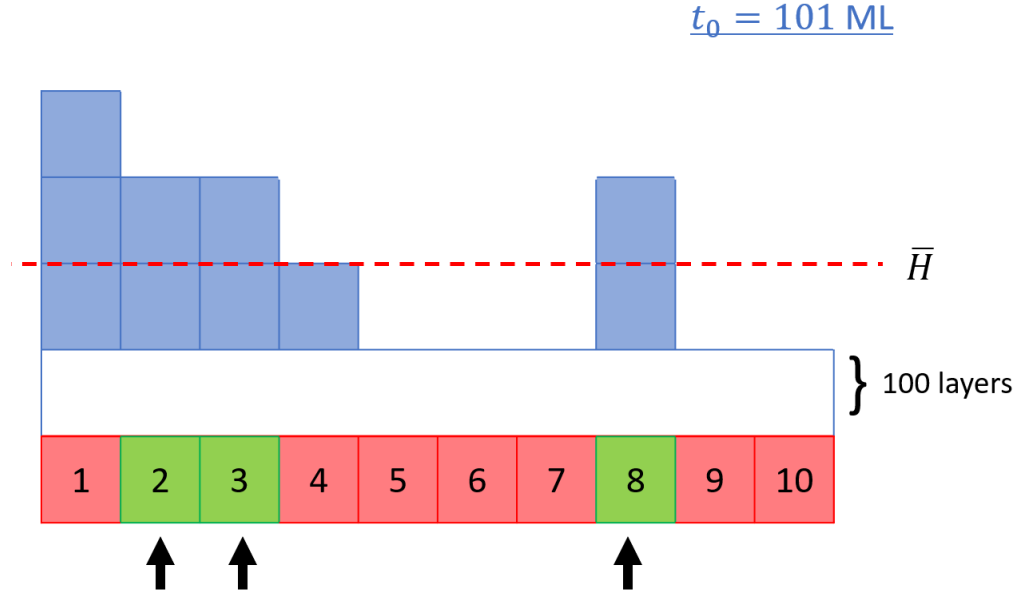
Figure 3.4: Diagram of persistence probability of a specific height fluctuation.

collected to $P_+^S(h_0 = 1)$ are determined by those with $h_0(t) > 1$ while sites included to $P_-^S(h_0 = 1)$ category are those with $h(t) < 1$.

The results of several linear models (Chanphana et al., 2013) as well as the non-linear DT model (Chanphana and Chatraphorn, 2021) show that the positive persistence probability of positive initial height fluctuation ($P_+^S(+|h_0|, t)$) and the negative persistence probability of negative initial height fluctuation ($P_-^S(-|h_0|, t)$) do not exhibit power law decay. The power law decay behavior of $P_\pm^S(h_0, t)$ are only found for the positive persistence probability of negative initial height fluctuation ($P_+^S(-|h_0|, t)$) and the negative persistence probability of positive initial height fluctuation ($P_-^S(+|h_0|, t)$). For the (2+1) dimensional DT model, $P_+^S(-|h_0|, t)$ exhibits power law decay when $h_0 \gg w_{sat}$ whereas the condition of $P_-^S(+|h_0|, t)$ is $h_0 \gtrsim w_{sat}$. In contrast, only the condition $h_0 \gtrsim w_{sat}$ to have the power law decay can be applied to $P_\pm^S(\mp|h_0|, t)$ for all linear models (Chanphana et al., 2013).

It is clear that $P_\pm^S(\pm|h_0|, t)$ do not display a power law decay because of the diffusion of the surface atoms. At the site with positive h_0, the height of that site is larger than the mean height at the time we measure. The only chance that the height of that site remains larger than the mean height is for the newly deposited atom to stick on top of it. So, $P_+^S(+|h_0|, t)$ generally decays very fast. The behavior of $P_-^S(-|h_0|, t)$ is the same as $P_+^S(+|h_0|, t)$. The height fluctuation of the site with negative h_0 will remain negative if no atom falls into the groove. Both events are relatively rare due to surface atom diffusion, leading to the quick decay of the probabilities and thus we do not study $P_\pm^S(\pm|h_0|, t)$ in this work.

In this thesis, we examine $P^S_\pm(t, L, \delta t, |h_0|)$ in the (2+1)-MBE model with different initial heights, system sizes and sampling times and follow the scaling relation reported in the literature (Chanphana et al., 2013; Chanphana and Chatraphorn, 2021).

จุฬาลงกรณ์มหาวิทยาลัย
CHULALONGKORN UNIVERSITY

Chapter IV

RESULTS

In chapter 4, all results are reported. We show effects of growth temperature on film morphology. Effects of growth temperature and deposition rate on persistence exponents are investigated. The persistence probabilities with various initial height fluctuation are studied. We obtain the initial height conditions in order to have a power law decrease in time for persistence probabilities of the MBE model. Scaling behavior of the persistence probability is explored.

We are aware that if we simulate a very small system size (L), the finite size effect will cause additional inaccuracies in the results. However, simulating a large system size would take a long time in order to eliminate this effect. The minimum system size chosen in this study is 50×50 sites, which is acceptable for the (2+1)-dimensional MBE model because finite size effect is small enough. We examine the scale invariance property through the simulation of thin films with various system sizes from 50×50 to 100×100 sites. The simulation time for 100×100 sites, which is the largest, is still reasonable.

4.1 Effects of temperature on interface width and persistence exponent

Plots of $w(t)$ at different temperature are shown in figure 4.1. The slope in the early stage (the black solid line) represents the value of β which obviously decreases as the temperature goes up. When T increases from 700 K to 750 K, the film interface saturates faster with smaller w_{sat}. Since w is the root mean square of the height fluctuation, w tells us how large that the height at each site differs from the averaged height. Smaller w_{sat} is an indication of a smoother surface at the steady-state.

The reason for a smoother film at higher growth temperature is in equation (2.5). From equation (2.5), increasing growth temperature (T) leads to the increase in diffusion length (l). This means as the temperature is increased, the atom can search further for the stable site to be incorporated, thus the film is smoother. At each temperature, the maximum value of l is l_{max} which is the diffusion length of the surface atoms with $n = 1$. Figure 4.2 shows that when the temperature rises from $T = 700$ K to $T = 750$ K, corresponding to the increase from $l_{max} = 1$ to $l_{max} = 5$, the surface morphology becomes much smoother.

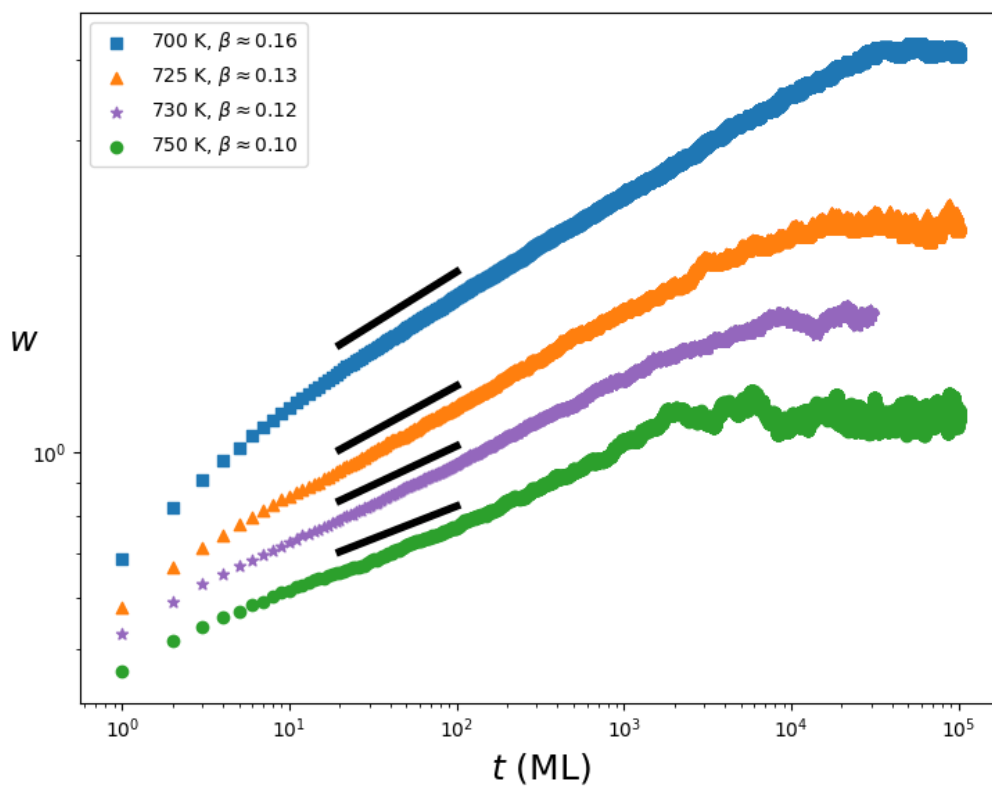It is worth pointing out that the morphology in figure 4.2(a) is quite simi-

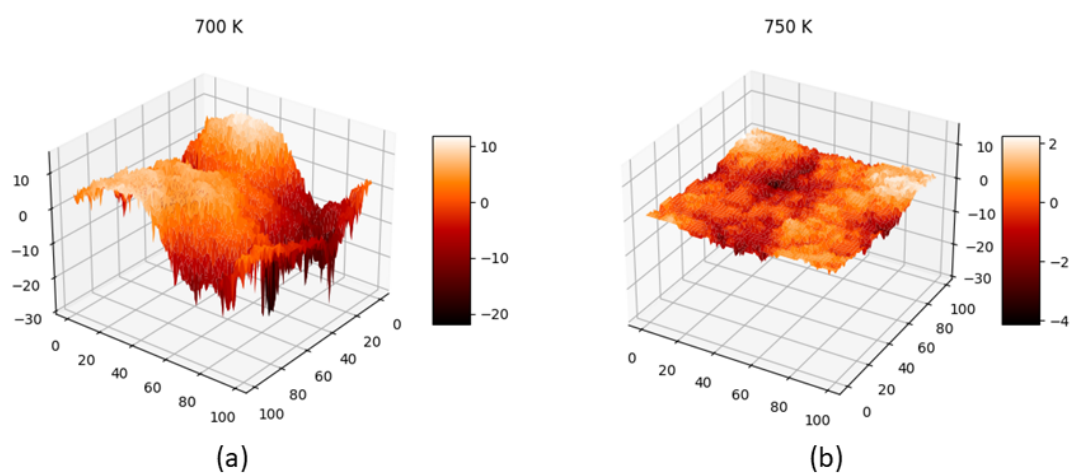Figure 4.1: $w(t)$ with varying temperature with $F = 1$ ML/s. Solid black lines are fitting lines for β.

Figure 4.2: Morphology of the MBE model with $L \times L = 100 \times 100$ sites at steady state with temperature: (a) $T = 700$ K ($l_{max} = 1$) and (b) $T = 750$ K ($l_{max} = 5$).
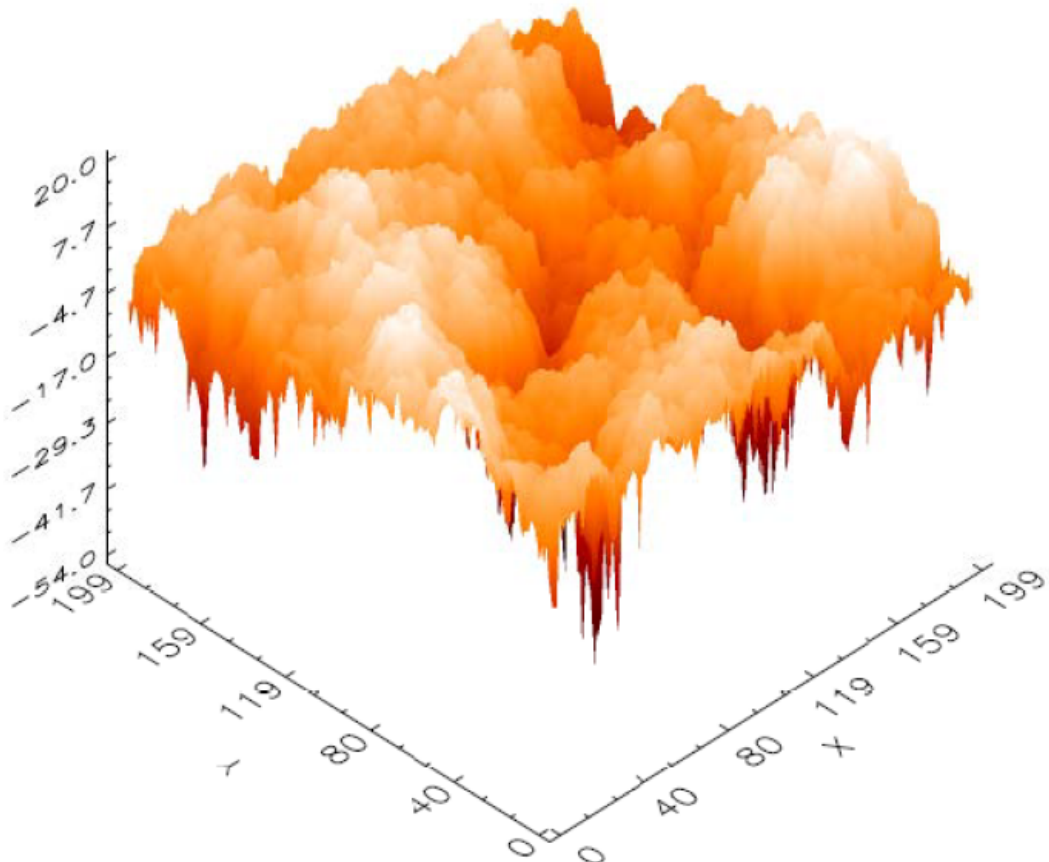
Figure 4.3: Morphology of the DT model with L×L=200×200 sites at steady state (Chanphana, 2013).

lar to that of the DT model (Das Sarma and Tamborenea, 1991; Tamborenea and Das Sarma, 1993) shown in figure 4.3 (Chanphana, 2013) with deep grooves and smooth top surface, so it is not surprising that the persistence probabilities of the MBE model have similar behavior to those of the DT model (Chanphana and Chatraphorn, 2021).

Plots of the persistence probabilities (averaged over all h_0) $P_{\pm}^{S}$ of varying temperature are shown in figure 4.4. When the film is smoother at high temperature, h returns to h_0 faster for a flatter surface. $P_{\pm}^{S}$, whose maximum values at $t = 1$ are normalized to be 1, decay faster for higher temperature. The value of $\theta_{\pm}^{S}$, which are the slope of the plots, then increase with the temperature. In conclusion, increasing T causes $P_{\pm}^{S}$ to decrease more quickly, resulting in an increase in $\theta_{\pm}^{S}$ as shown in figure 4.4.

The value of $\theta_{\pm}^{S}$ are calculated by averaging among all independent simulation systems. The standard deviation of the mean is used as the error of $\theta_{\pm}^{S}$. In our results, the errors are very small. For instance, the standard error of θ_{+}^{S} at $T = 700$ K for

the substrate size $L \times L = 100 \times 100$ sites, averaged of 1,860 independent runs, is 2.76×10^{-3}. The error of other systems are also not greater than the order of 10^{-3}. Thus, we do not show the error bars in our graphs. Note that the errors of β are in the same order.
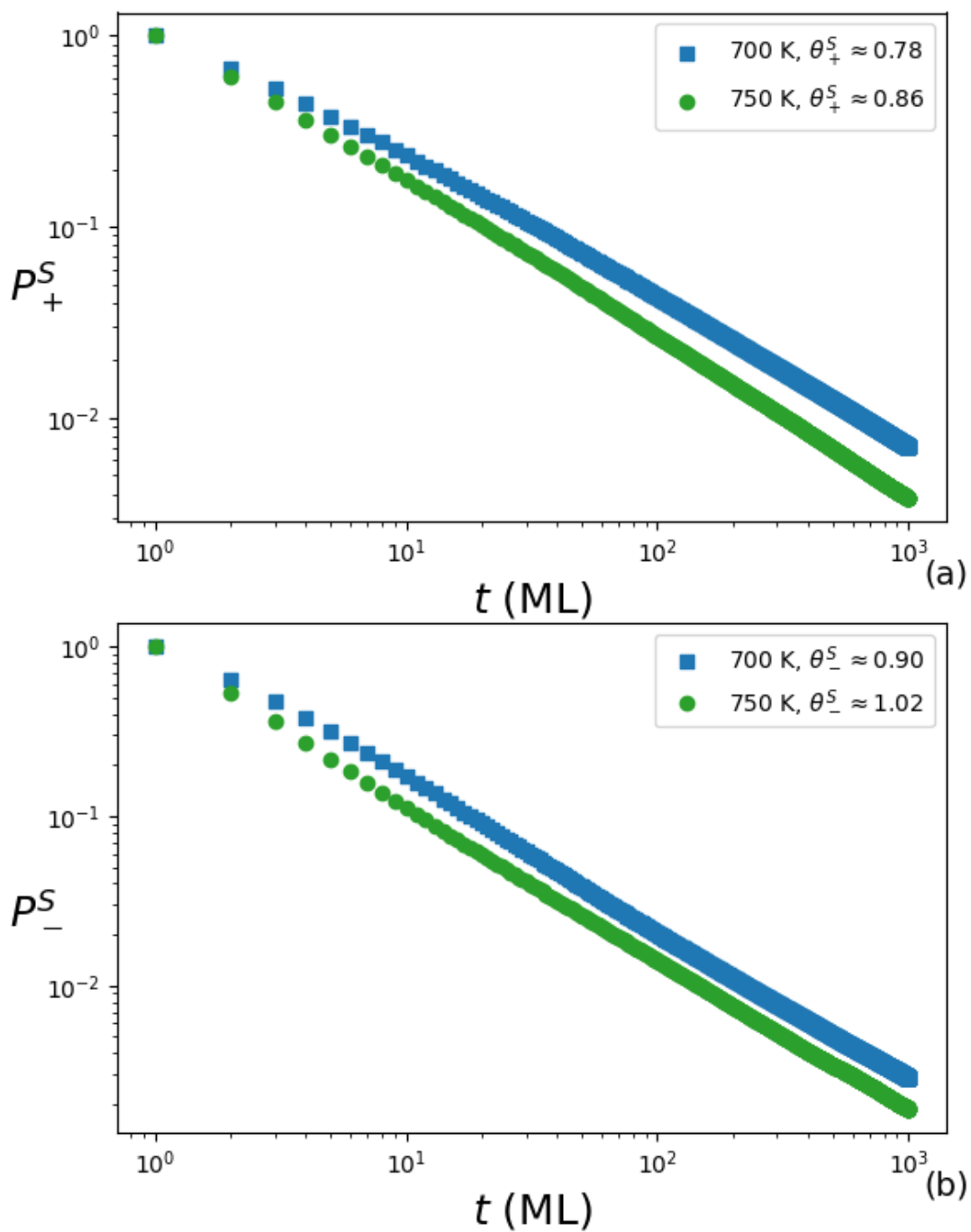
Figure 4.4: (a) $P_+^S(t)$ and (b) $P_-^S(t)$ with two different temperatures. θ_+^S and θ_-^S are calculated from the slope in the range of $t = 100 - 400$ ML.

4.2 Effects of deposition rate on interface width and persistence exponent

Deposition rate and temperature have completely opposite effects on interface growth. When we increase the deposition rate, more atoms arrive at the surface in a short time interval so each atom has a very limited period of time to diffuse, which results in a short diffusion length. There will not be any diffusion if F is too large. Atoms will stick to their landing sites, creating very rough film surface. In that case, the interface evolves in the same way as the RD model. In contrast, a slow deposition rate provides more deposition time as indicated from eq. (2.1). As a result, the diffusion length is long because atoms have more time to diffuse. This process agrees with the experimental study that reduced deposition rate helps to smoothen the film morphology (Maboudian et al., 1994).

Figure 4.5 shows plots of l vs T for various values of F $(0.33, 0.5, 1$ and 2 ML/ s) of the atoms that only share one bond with the substrate. For each value of F, increasing in temperature results in an increase in diffusion length. The graph will shift to the right when F rises. When fixing T, larger F causes the drop in l. Because l can only be an integer, the graphs are discontinuous.

A slower rate of deposition, which is associated with an increase in temperature, leads to the smoother surface morphology. From the previous section, $T = 700, 725, 730$ and 750 K with $F = 1$ ML/s in figure 4.1 correspond to $F = 1, 0.5, 0.33$ and 0.2 ML/s with $T = 700$ K, respectively. Plots of w vs t show the decrease in β as F decreases (T increases). The results of $P_{\pm}^{S}(t)$ with varying deposition rates are shown in figure 4.6. $P_{\pm}^{S}(t)$ are found to decay more slowly with larger F that cause rougher surface.

As was previously mentioned, the standard error of $\theta_{\pm}^{S}$ with varying deposition rates are in the order of 10^{-3}, we conclude that the $\theta_{\pm}^{S}$ for different deposition rates are not equal to each other within the error bar.

We report our results of β and $\theta_{\pm}^{S}$ with varying the diffusion length in table 4.1. For the MBE model, we obtain $\theta_{+}^{S} < \theta_{-}^{S}$ for every condition. The relation $\beta = max\left[1 - \theta_{+}^{S}, 1 - \theta_{-}^{S}\right]$ in equation (3.2) suggests that in this model, $\beta_{eq\,3.2} = 1 - \theta_{+}^{S}$. Due to the substrate size limitation and simulation time restriction, β obtained in figure 4.1 slightly differs from $\beta_{eq\,3.2} = 1 - \theta_{+}^{S}$. However, the value of β from figure 4.1 is closer to $1 - \theta_{+}^{S}$ than $1 - \theta_{-}^{S}$. Thus, our findings support the theory that β remains related to the smaller persistence exponent.
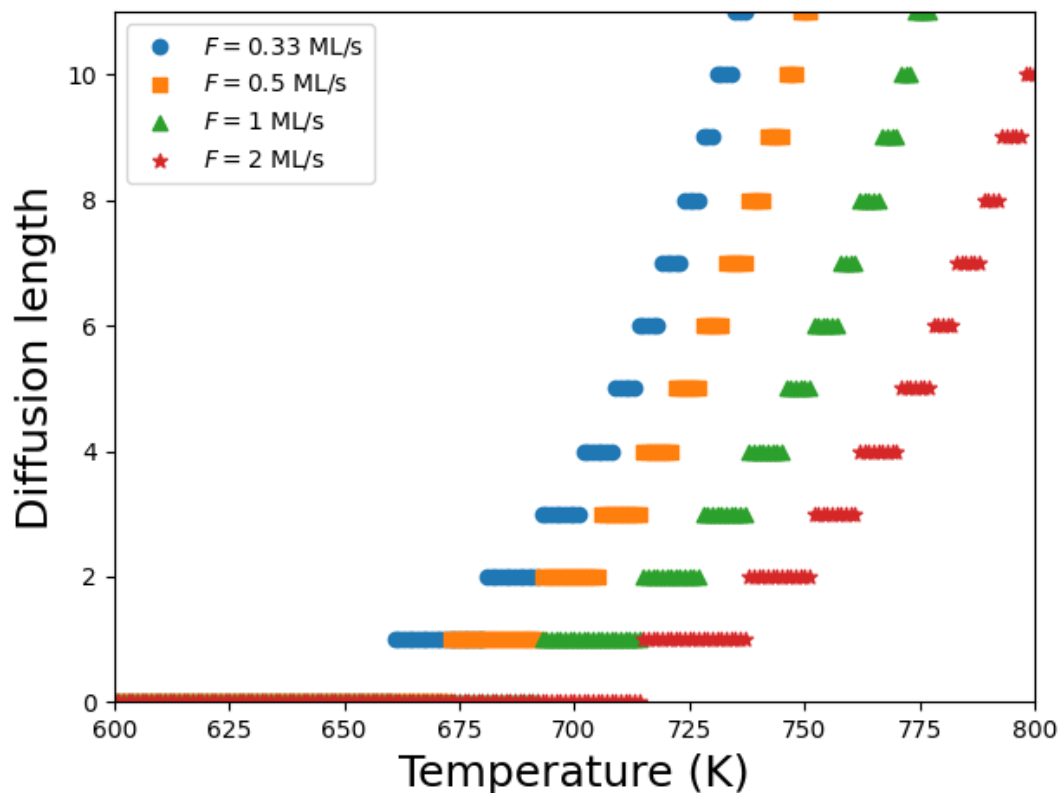
Figure 4.5: Diffusion length plotted against temperature, with varying the deposition rate for the surface atom with $n = 1$.

Parameters	Values				Conditions
l_{max}	1	2	3	5	
T (K)	700	725	730	750	$F = 1$ ML/s
F (ML/s)	1	0.5	0.33	0.2	$T = 700$ K
β	0.16	0.14	0.12	0.10	
θ_+^S	0.78	0.82	0.84	0.86	
θ_-^S	0.90	0.93	0.97	1.02	
$\beta_{eq\,3.2} = max[1 - \theta_+^S, 1 - \theta_-^S]$	0.22	0.18	0.16	0.12	

Table 4.1: A summary table of approximate value of β and $\theta_\pm^S$ under different conditions.
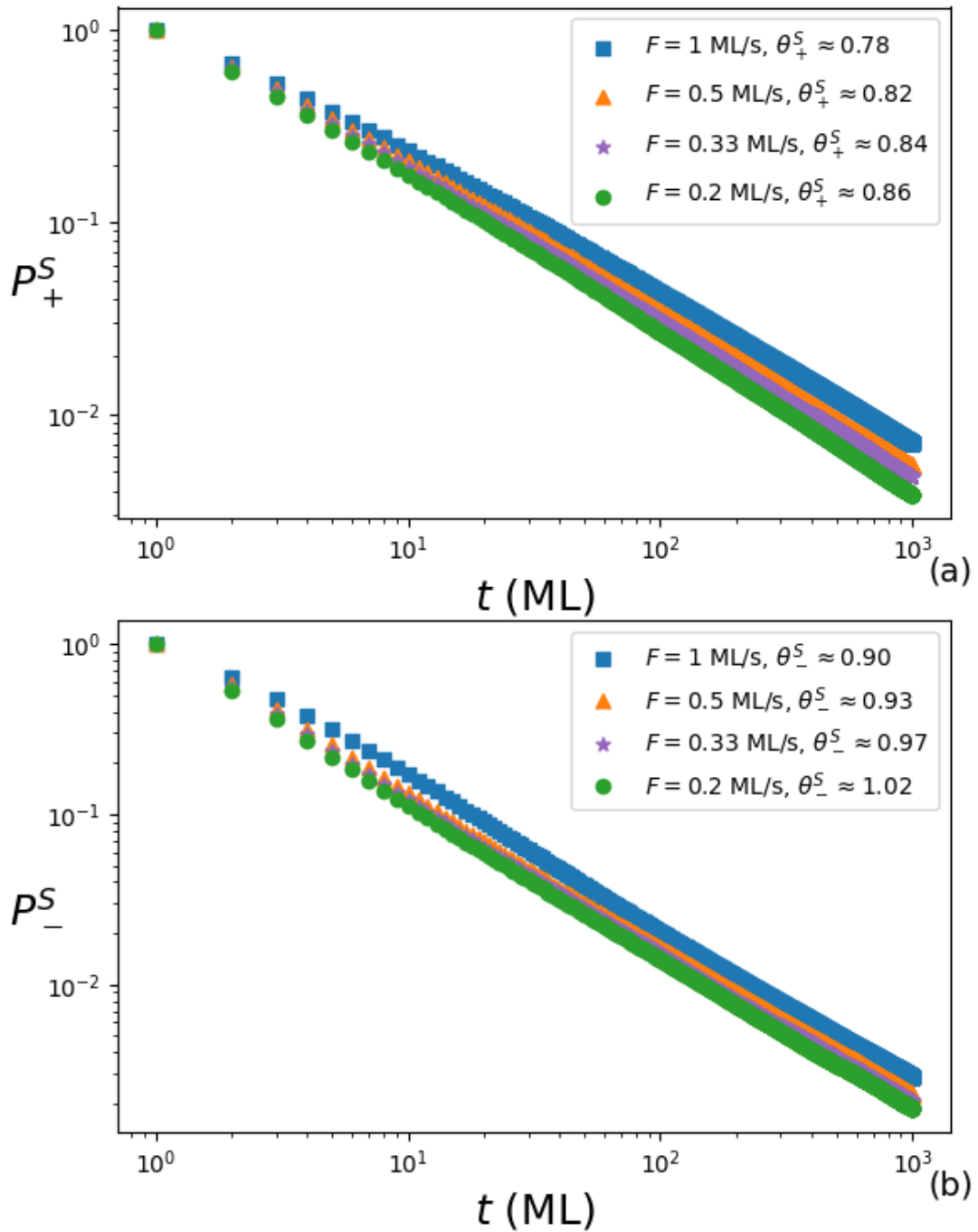
Figure 4.6: (a) $P^S_+(t)$ and (b) $P^S_-(t)$ with different deposition rates. θ^S_+ and θ^S_- are calculated from the slope in the range of $t = 100 - 400$ ML.

4.3 Effects of initial height fluctuations on persistence exponent

From chapter 3, we discuss effects of h_0 on $P_\pm^S(t)$ and results from the previous studies (Chanphana et al., 2013; Chanphana and Chatraphorn, 2021) which suggest that $P_\pm^S(h_0, t)$ only exhibit power law decay in time under some specific situation. We neglect $P_\pm^S(\pm|h_0|, t)$ because of their rapid decay and lack of power law behavior. Our simulation results for the MBE model show that the positive persistence probability of negative initial height fluctuation ($P_+^S(-|h_0|, t)$) exhibits the desired power law decay only when $|h_0| \gg w_{sat}$. In contrast, the negative persistence probability of positive initial height fluctuation ($P_-^S(+|h_0|, t)$) shows the power law decay when $|h_0| \gtrsim w_{sat}$. Figure 4.7 (a) and (b) show plots of $P_+^S(-|h_0|, t)$ and $P_-^S(+|h_0|, t)$ of the system size $L \times L = 50 \times 50$ sites with $w_{sat} \approx 2.90$. It can be seen that at $|h_0| = 4$, the plot of $P_+^S(-|h_0|, t)$ in figure 4.7 (a) does not exhibit a power law decline whereas the plot of $P_-^S(+|h_0|, t)$ in figure 4.7 (b) clearly does. From figure 4.7 (a), only P_+^S of very large $|h_0|$, i.e., $|h_0| \gtrsim 10$ shows an approximate straight line in the log-log scale. Moreover, we observe that both $P_+^S(-|h_0|, t)$ and $P_-^S(+|h_0|, t)$ with larger value of $|h_0|$ undergo slower rate of decrease in time when compared to those with smaller $|h_0|$. This result indicates that stronger fluctuations on the film surface persist longer than weaker ones.

Effects of h_0 on $P_+^S(t)$ of the (2+1)-DT model with $l = 1$ are investigated in (Chanphana and Chatraphorn, 2021). Their plots of $P_+^S(-|h_0|, t)$ as a function of any h_0 are shown in figure 4.8. Their results are from simulations with $L \times L = 100 \times 100$ where $w_{sat} \approx 6.87$. For the DT model, $P_+^S(-|h_0|, t)$ exhibits power law decay when $|h_0|17$ which is significantly larger than w_{sat}. Our results of $P_-^S(+|h_0|, t)$ are also comparable to those of the DT model. As a result, our finding of conditions for a power law decay behavior in $P_\pm^S(\mp|h_0|, t)$ of the MBE model are similar to those of the DT model (Chanphana and Chatraphorn, 2021).
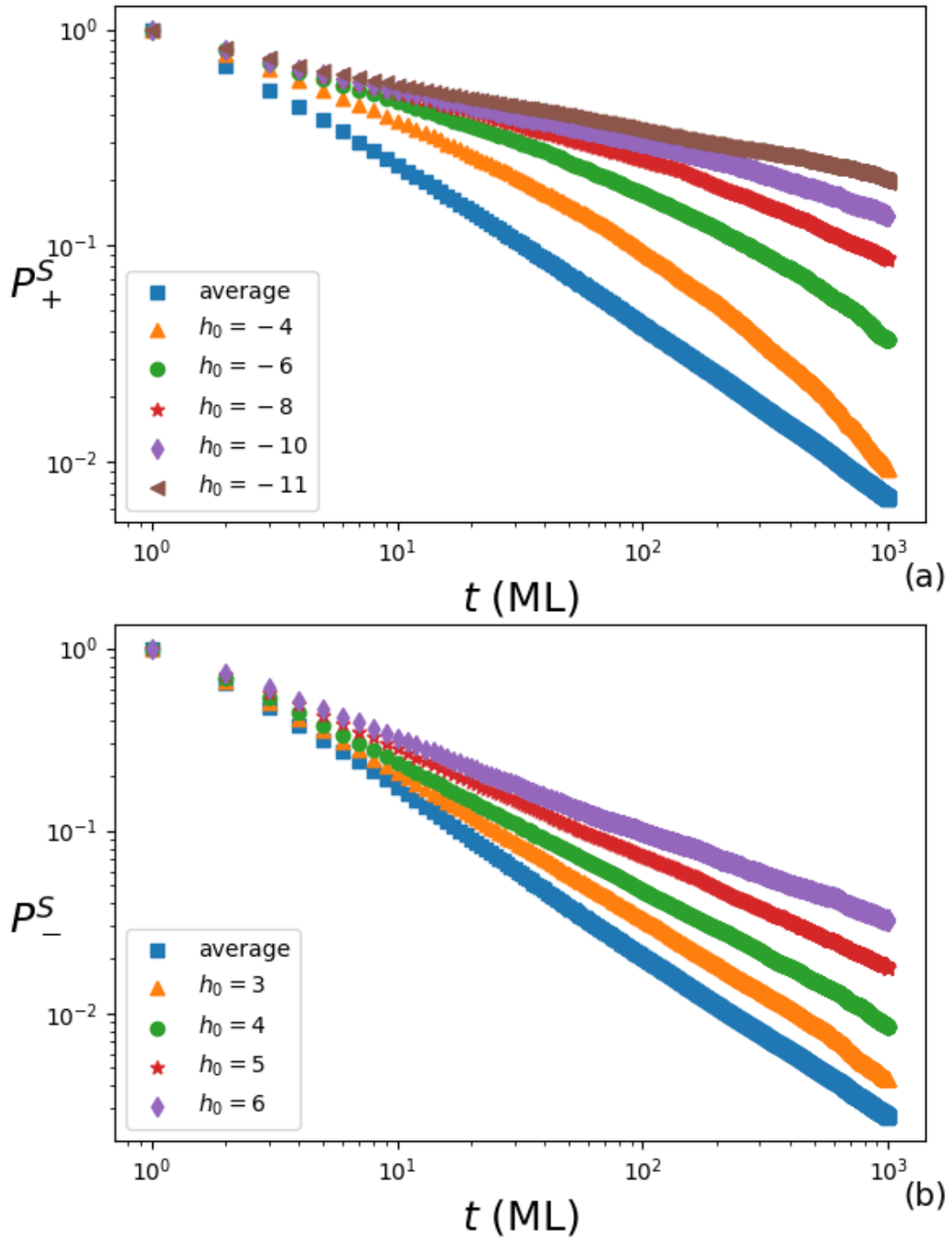
Figure 4.7: (a) $P_+^S(-|h_0|, t)$ and (b) $P_-^S(+|h_0|, t)$ with varying h_0 from the system $L \times L = 50 \times 50$ sites.
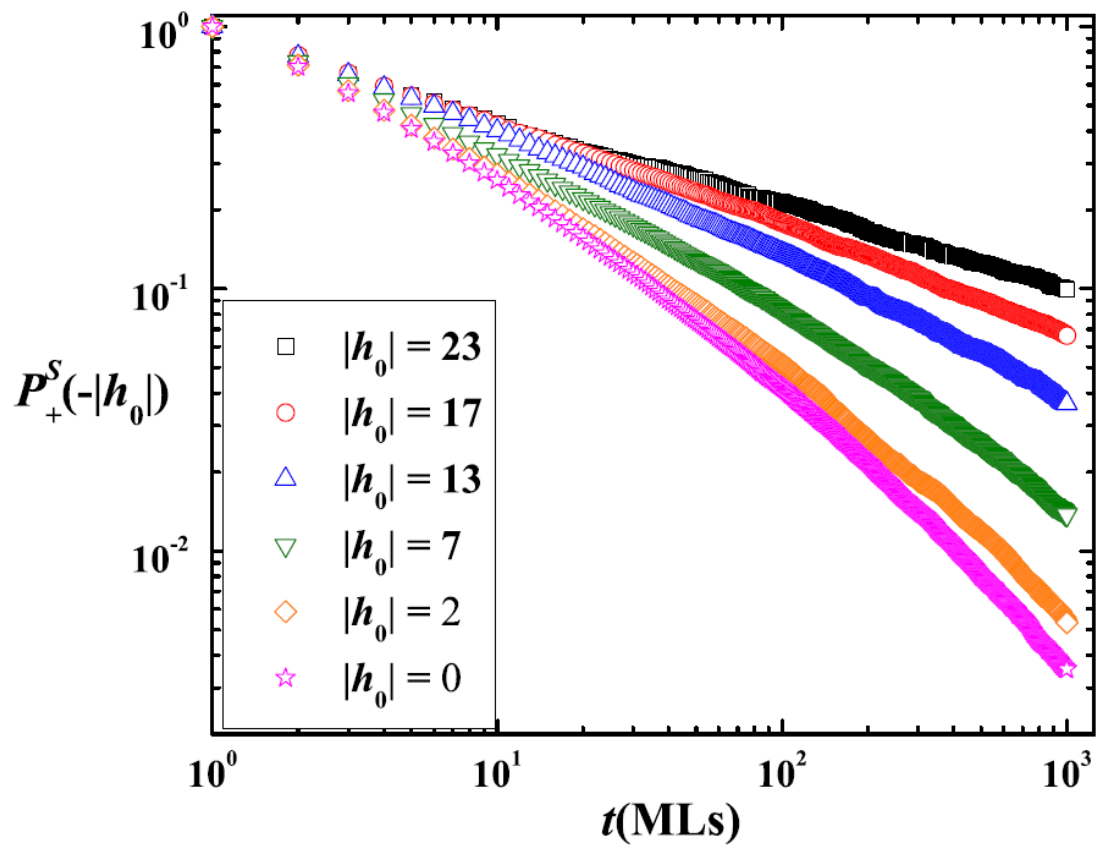
Figure 4.8: $P_+^S(-|h_0|, t)$ with varying h_0 of (2+1)-dimensional DT model (Chanphana, 2013).

4.4 Effects of discrete sampling time on persistence probability

We investigate effects of the discrete sampling time, δt, on $P_\pm^S(t)$ in the MBE model. The system size used here is $L \times L = 50 \times 50$ sites with $l_{max} = 1$. Figures 4.9 (a) and (b) show plots of $P_+^S(t)$ and $P_-^S(t)$ with varying δt. The values of δt used are 1, 2 and 4. It can be seen from the figures that at a specific time t, the value of $P_\pm^S(t)$ is greater for larger δt. Despite the different values in the persistence probabilities, all $P_+^S(t)$ plots approximately decay with the same rate. The same behaviors are seen in $P_-^S(t)$. These results are consistence with (Constantin et al., 2004b; Dougherty et al., 2005).

จุฬาลงกรณ์มหาวิทยาลัย
CHULALONGKORN UNIVERSITY

Figure 4.9: (a) $P_+^S(\delta t, t)$ and (b) $P_-^S(\delta t, t)$ with varying δt from the system size $L \times L = 50 \times 50$ sites.
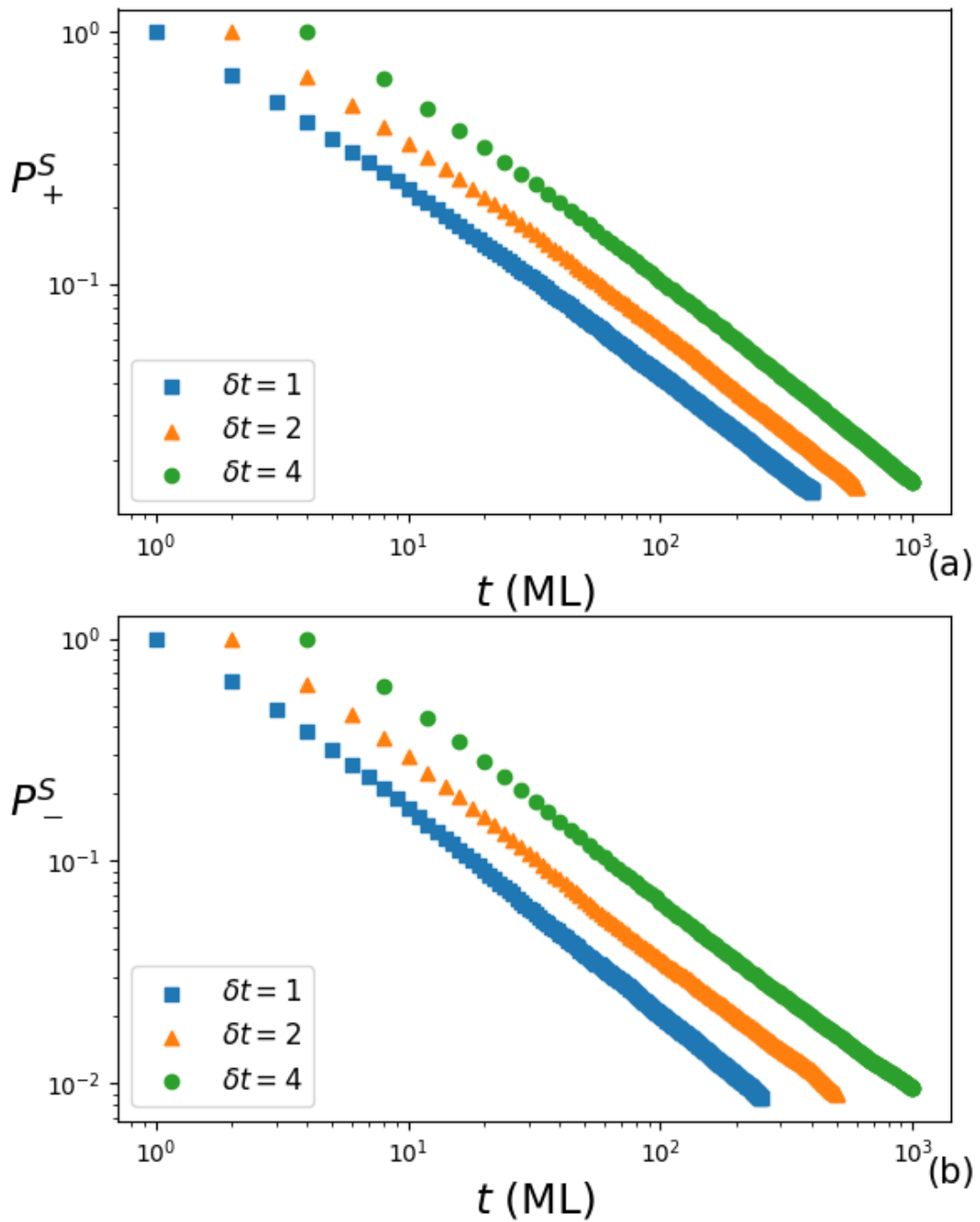
4.5 Scaling behavior of persistence probability

Investigating $P_{\pm}^S$ of a specific value of h_0, we find that $P_{-}^S(+|h_0| \gtrsim w_{sat}, t)$ and $P_{+}^S(-|h_0| \gg w_{sat}, t)$ present power law decay. Next, we examine their scaling behavior. Since the morphology of the MBE model shown in figure 4.2 and results of $P_{\pm}^S(h_0, t)$ in figure 4.7 are consistent with those of the DT model, we assume the possibility of $P_{\pm}^S(h_0)$ to have the same scaling relation as shown in Chanphana and Chatraphorn (Chanphana and Chatraphorn, 2021) for the MBE model.

Temporal part scales the same for P_{+}^S and P_{-}^S as we discuss in chapter 3. Since the saturation time scales with the substrate size as L^z where z is the dynamical exponent, δt should scale with L^z as well. Additionally, when L is varied, w_{sat} and range of possible h_0 are changed. From these behaviors, the other expected scaling ratio is $|h_0|/w_{sat}$. In this work, we fix the diffusion length condition to be $l = 1$, and the dynamical exponent of the MBE model for $l = 1$ is $z = 3.3$. $P_{-}^S(+|h_0|, t)$ and $P_{+}^S(-|h_0|, t)$ with different L, δt and h_0, but fixed ratios $\delta t/L^z$ and $|h_0|/w_{sat}$ for each system size are plotted in figures 4.10 and 4.11. The minimum system size is 50×50 sites, and δt is chosen to be 1 for this substrate size. So, the ratio, which is also used for the other L, is $\delta t/L^z \approx 2.47 \times 10^{-6}$. For $P_{-}^S(+|h_0|, t)$, we choose $h_0 = 4$ and the scaling ratio is $|h_0|/w_{sat} \approx 1.38$. For $P_{+}^S(-|h_0|, t)$, we choose $h_0 = -10$ with $|h_0|/w_sat \approx 3.48$. Once again, for every L, the ratio $|h_0|/w_{sat}$ is fixed. However, since δt and h_0 cannot be a fraction, both ratios which are supposed to be constant for all L, are only approximately constant with the percentage difference of less than 6%. After rescaling all plots with δt, the probabilities in figures 4.10 and 4.11 roughly collapse into a single curve. These results confirm that the persistence probabilities of the MBE model follow the relation established in prior researches (Chanphana et al., 2013; Chanphana and Chatraphorn, 2021).

Since $w_{sat} \sim L^\alpha$, the ratio $|h_0|/w_{sat}$ can be written in terms of the roughness exponent as $|h_0|/L^\alpha$. In summary, $P_{\pm}^S(t, L, \delta t, |h_0|)$ are the function of $f(t/L^z, \delta t/L^z, |h_0|/L^\alpha)$, where t/L^z 1, $\delta t/L^z \ll 1$ and $|h_0|/L^\alpha > 1$.

Figure 4.10: (a) $P_-^S(+|h_0|, t)$ with different $\delta t, h_0$ and L. The fixed ratios are $\delta t/L^z \approx 2.47 \times 10^{-6}$ and $|h_0|/w_{sat} \approx 1.41$. (b) Scaling collapse of $P_-^S(t, L, \delta t, |h_0|)$.
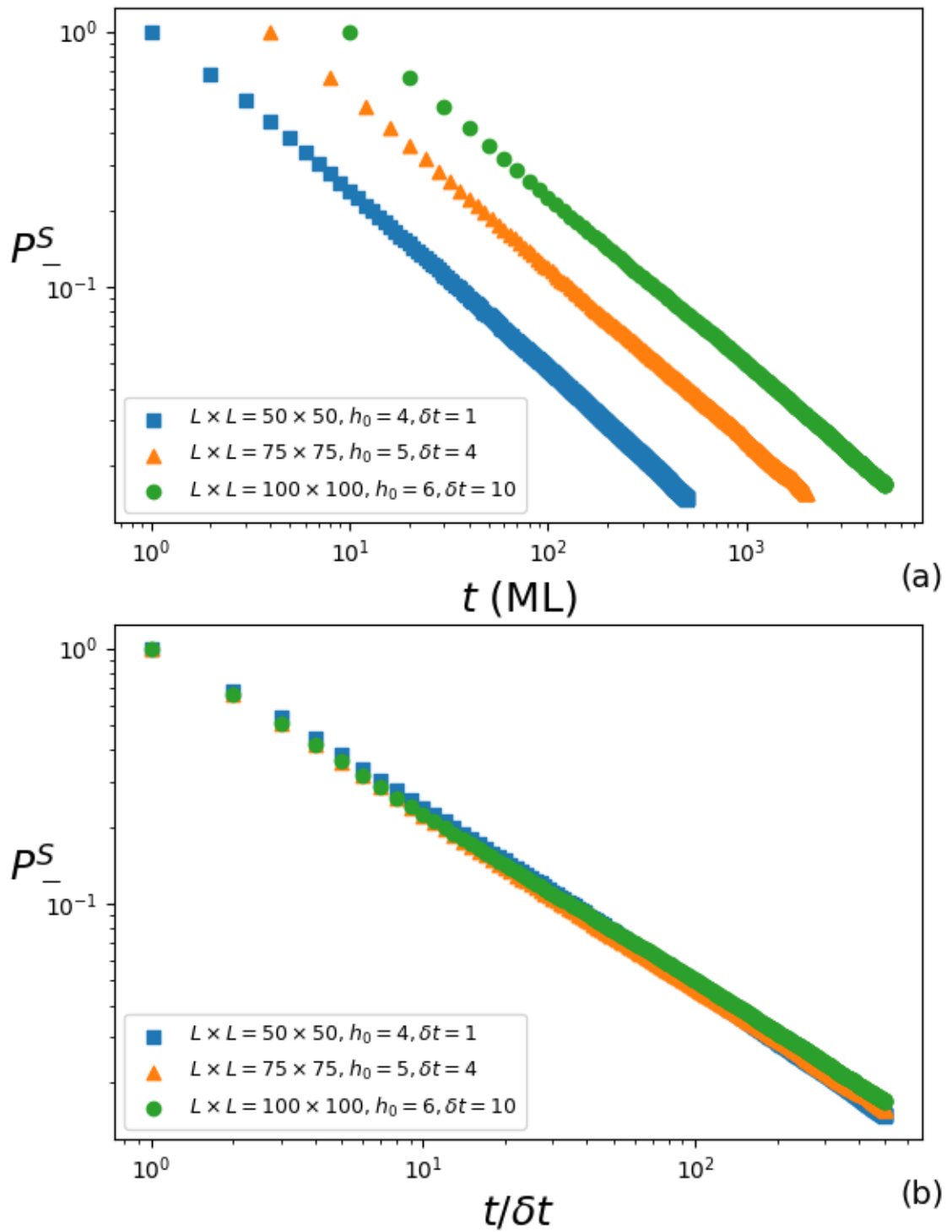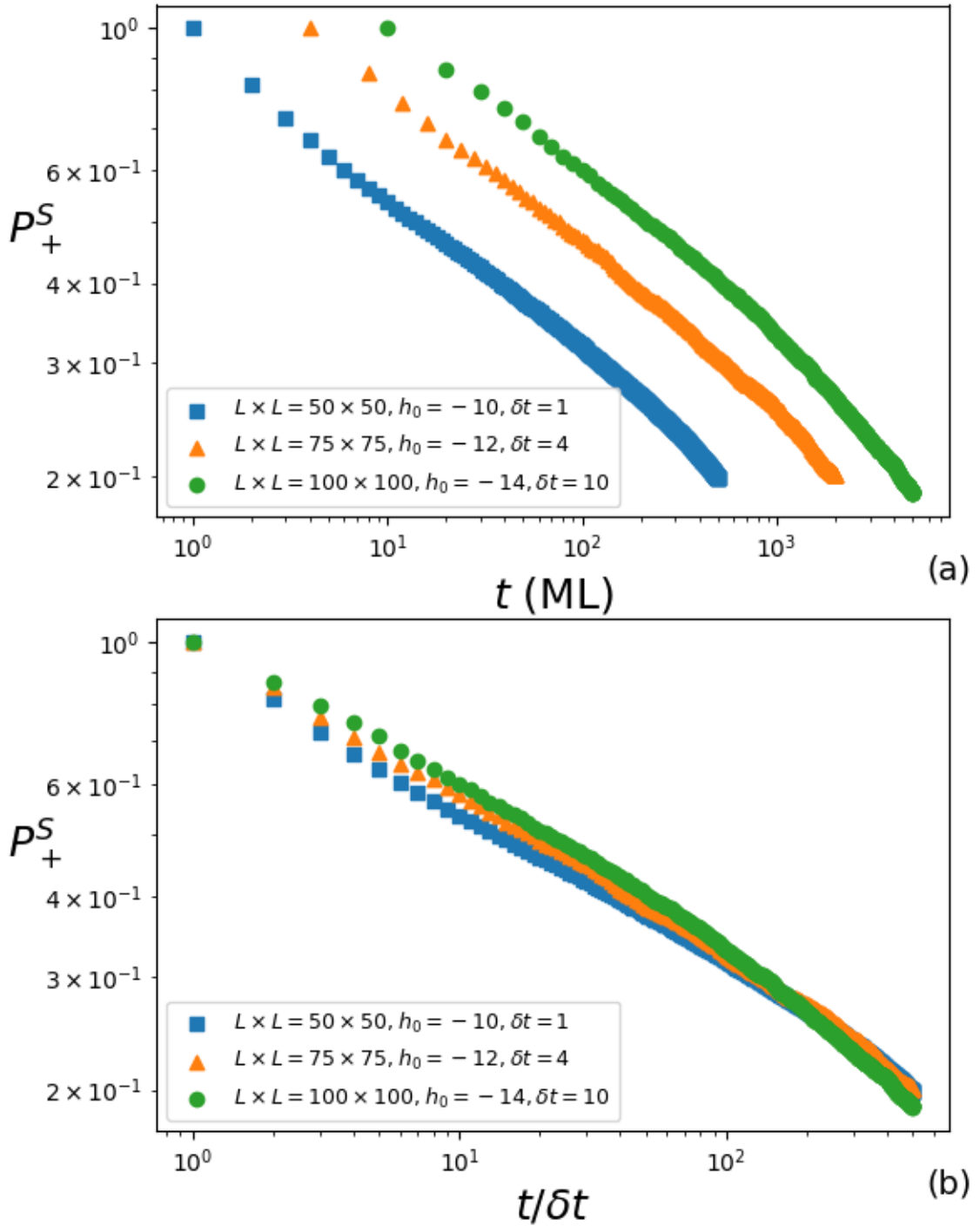
Figure 4.11: (a) $P_+^S(-|h_0|, t)$ with different $\delta t, h_0$ and L. The fixed ratios are $\delta t / L^z \approx 2.47 \times 10^{-6}$ and $|h_0| / w_{sat} \approx 3.40$. (b) Scaling collapse of $P_+^S(t, L, \delta t, |h_0|)$.

Chapter V

CONCLUSIONS

Our results show that the MBE model is up-down asymmetric due differences in morphology between upward (positive h) and downward (negative h) directions. Deep grooves and rounded top surfaces are produced by the surface atom diffusion rules. The outcome of this asymmetry is that P_+^S and P_-^S decrease at different rate i.e. $\theta_+^S \neq \theta_-^S$. Both growth stages result in $\theta_+ < \theta_-$ which tell us that the positive height fluctuation has a longer time span than the negative one before crossing the initial value. In theory, the up-down asymmetry is represented by non-linear terms in the continuum equation.

Variation in temperature and deposition rates cause the change in diffusion length. The diffusion length grows with temperature while reducing as deposition rate rises. As l increases, film becomes smoother. This causes the decrease in β but the increase in $\theta_\pm^S$. The relation of β and $\theta_\pm^S$ with different diffusion lengths follows equation (3.2) derived by Constantin and coworkers (Constantin et al., 2004b).

We investigate effect of specific h_0 on $P_\pm^S(\mp|h_0|, t)$. We ignore $P_\pm^S(\pm|h_0|, t)$ because they do not exhibit power law decay. We find that the conditions to have the power law decay are $|h_0|/w_{sat} \gtrsim 1$ for $P_-^S(+|h_0|, t)$ and $|h_0|/w_{sat} \gg 1$ for $P_+^S(-|h_0|, t)$. For $P_-^S(+|h_0|, t)$, the sites of moderate value of $+|h_0|$ are the sites whose atoms sit on top of a small hill. They easily depart from their initial position during diffusion, so h of those sites remain less than h_0. This scenario leads to nonzero persistence probability of those sites. So, plots of $P_-^S(+|h_0| \gtrsim w_{sat}, t)$ does not drop too fast but decrease as a power law with time. For $P_+^S(-|h_0|, t)$ with extremely large $-|h_0|$, they are the sites whose atoms locate at the bottom of the groove. The groove can be easily filled by diffusing atoms, h remains greater than h_0 leading to nonzero P_+^S of those sites. So, plots of $P_+^S(-|h_0|, t)$ where $|h_0| \gg w_{sat}$ show a power law decay.

In order to find the scaling form of the persistence probabilities, we simulate $P_\pm^S(\mp|h_0|, t)$ for three sets of $(L, \delta t, |h_0|)$ with the ratios $\delta t/L^z$ and $|h_0|/w_{sat}$ are fixed. Plots of $P_\pm^S(t, L, \delta t, |h_0|)$ approximately collapse into a single line after rescaling t with δt. As $w_{sat} \sim L^\alpha$, $P_\pm^S$ are a function of $f(t/L^z, \delta t/L^z, |h_0|/L^\alpha)$, which is in agreement with those in earlier researches (Chanphana et al., 2013; Chanphana and Chatraphorn, 2021).

REFERENCES

Arthur Jr, J. 1968. Interaction of ga and as2 molecular beams with gaas surfaces. Journal of Applied Physics 39 (1968): 4032–4034.

Aurzada, F. and Kilian, M. 2022. Asymptotics of the persistence exponent of integrated fractional brownian motion and fractionally integrated brownian motion. Theory of Probability & Its Applications 67.1 (2022): 77–88.

Aurzada, F. and Simon, T. 2015. Persistence probabilities and exponents. In Lévy matters V, pp. 183–224. : Springer.

Ballestad, A., Ruck, B., Adamcyk, M., Pinnington, T., and Tiedje, T. 2001. Evidence from the surface morphology for nonlinear growth of epitaxial gaas films. Physical review letters 86 (2001): 2377.

Barabási, A.-L. and Stanley, H. E. 1995. Fractal concepts in surface growth. Cambridge university press.

Barnett, S. A. and Rockett, A. 1988. Monte carlo simulations of si (001) growth and reconstruction during molecular beam epitaxy. Surface science 198 (1988): 133–150.

Chanphana, R. and Chatraphorn, P. 2019a. Effects of surface diffusion length on steady-state persistence probabilities. In Journal of Physics: Conference Series, volume 1380, p. 012024. :

Chanphana, R. and Chatraphorn, P. 2019b. Generalized survival probabilities in height fluctuations of limited mobility growth models with and without up–down symmetry. Journal of Statistical Physics 176 (2019): 932–945.

Chanphana, R. and Chatraphorn, P. 2021. Persistence probabilities of height fluctuation in thin film growth of the das sarma–tamborenea model. Indian Journal of Physics 95 (2021): 187–193.

Chanphana, R., Chatraphorn, P., and Dasgupta, C. 2013. Effects of initial height on the steady-state persistence probability of linear growth models. Physical Review E 88 (2013): 062402.

Chanphana, R. 2013. Persistence probabilities of height fluctuation in thin film growth using discrete models with up-down symmetry. PhD thesis, Chulalongkorn University.

Constantin, M., , S., Das Sarma., and Dasgupta, C. 2004a. Spatial persistence and survival probabilities for fluctuating interfaces. Physical Review E 69 (2004): 051603.

Constantin, M., Dasgupta, C., Chatraphorn, P. P., Majumdar, S. N., and Das Sarma, S. 2004b. Persistence in nonequilibrium surface growth. Physical Review E 69 (2004): 061608.

Das Sarma, S. 1996. Growth models for virtual molecular beam epitaxy. Computational Materials Science 6 (1996): 149–157.

Das Sarma, S. and Tamborenea, P. 1991. A new universality class for kinetic growth: One-dimensional molecular-beam epitaxy. Physical review letters 66 (1991): 325.

Dougherty, D., Lyubinetsky, I., Williams, E., Constantin, M., Dasgupta, C., and Das Sarma, S. 2002. Experimental persistence probability for fluctuating steps. Physical review letters 89 (2002): 136102.

Dougherty, D., Tao, C., Bondarchuk, O., Cullen, W., Williams, E., Constantin, M., Dasgupta, C., and Das Sarma, S. 2005. Sampling-time effects for persistence and survival in step structural fluctuations. Physical Review E 71 (2005): 021602.

Efraim, Y. and Taitelbaum, H. 2011. Persistence in reactive-wetting interfaces. Physical Review E 84.5 (2011): 050602.

Family, F. 1986. Scaling of rough surfaces: Effects of surface diffusion. Journal of Physics A: Mathematical and General 19 (1986): L441.

Family, F. and Vicsek, T. 1985. Scaling of the active zone in the eden process on percolation networks and the ballistic deposition model. Journal of Physics A: Mathematical and General 18 (1985): L75.

Fornari, C. I., Fornari, G., Paulo, H. d. O., Abramof, E., and dos Travelho, J. 2018. Monte carlo simulation of epitaxial growth. Epitaxy; Zhong, M., Ed.; BoD–Books on Demand: Norderstedt, Germany (2018): 113.

Franchi, S. 2013. Molecular beam epitaxy: fundamentals, historical background and future prospects. In Molecular Beam Epitaxy, pp. 1–46. : Elsevier.

Guan, F., Jiang, W., Li, G., Jiang, H., Zhu, J., and Fan, Z. 2019. Interfacial bonding mechanism and pouring temperature effect on al/cu bimetal prepared by a novel compound casting process. Materials Research Express 6.9 (2019): 096529.

Holloway, P. H. and McGuire, G. E. 2008. Handbook of compound semiconductors: growth, processing, characterization, and devices. Cambridge University Press.

Hotta, T., Takase, K., Takiguchi, K., Sriharsha, K., Anh, L. D., and Tanaka, M. 2022. Growth and characterization of quaternary-alloy ferromagnetic semiconductor (in, ga, fe) sb. AIP Advances 12 (2022): 015307.

Kazantsev, D., Akhundov, I., Karpov, A., Shwartz, N., Alperovich, V., Terekhov, A., and Latyshev, A. 2015. Monte carlo simulation of gaas (0 0 1) surface smoothing in equilibrium conditions. Applied Surface Science 333 (2015): 141–146.

Kellogg, G., Tsong, T., and Cowan, P. 1978. Direct observation of surface diffusion and atomic interactions on metal surfaces. Surface Science 70 (1978): 485–519.

Kittel, C. 2010. Introduction to solid state physics (japanese 8th-edition). Appendix I, Maruzen in Tokyo (2010):

Koguchi, N., Takahashi, S., and Chikyow, T. 1991. New mbe growth method for insb quantum well boxes. Journal of crystal growth 111 (1991): 688–692.

Krug, J. and Meakin, P. 1990. Universal finite-size effects in the rate of growth processes. Journal of Physics A: Mathematical and General 23 (1990): L987.

Krug, J., Kallabis, H., Majumdar, S., Cornell, S., Bray, A., and Sire, C. 1997. Persistence exponents for fluctuating interfaces. Physical Review E 56 (1997): 2702.

Lai, Z.-W. and Das Sarma, S. 1991. Kinetic growth with surface relaxation: Continuum versus atomistic models. Physical review letters 66 (1991): 2348.

Léonard, F., Laradji, M., and Desai, R. C. 1997. Molecular beam epitaxy in the presence of phase separation. Physical Review B 55 (1997): 1887.

Liang, K., Sun, X., Wu, G., Zhang, L., Liu, S., and Gan, Z. 2020. The investigation of molecular beam epitaxy growth of gan by molecular dynamics simulation. Computational Materials Science 173 (2020): 109426.

Luis, E. E. M., de Assis, T. A., Ferreira, S. C., and Andrade, R. F. 2019. Local roughness exponent in the nonlinear molecular-beam-epitaxy universality class in one dimension. Physical Review E 99 (2019): 022801.

Maboudian, R., Bressler-Hill, V., Pond, K., Wang, X.-S., Petroff, P., and Weinberg, W. 1994. Effect of growth rate on the surface morphology of mbe-grown gaas (001)-(2× 4). Surface science 302 (1994): L269–L274.

Majumdar, S. N. and Bray, A. J. 2001. Spatial persistence of fluctuating interfaces. Physical Review Letters 86.17 (2001): 3700.

Majumdar, S., Bray, A., Cornell, S., and Sire, C. 1996. Global persistence exponent for nonequilibrium critical dynamics. Physical review letters 77.18 (1996): 3704.

Marconi, D., Colniţă, A., and Turcu, I. 2016. The influence of deposition rate on the structure and morphology of gold/silicon (111) growth by molecular beam epitaxy. Analytical Letters 49.3 (2016): 400–410.

Morresi, L. 2013. Molecular beam epitaxy (MBE). Bentham Science Publishers Bussum.

Pal, S. and Landau, D. 1994. Monte carlo simulation and dynamic scaling of surfaces in mbe growth. Physical Review B 49 (1994): 10597.

Rangel-Kuoppa, V.-T., Ye, S., Noori, Y. J., Holmkvist, W., Young, R. J., and Muenstermann, D. 2021. Towards gaas thin-film tracking detectors. Journal of Instrumentation 16 (2021): P09012.

Ren, F. and Zheng, B. 2003. Generalized persistence probability in a dynamic economic index. Physics Letters A 313.4 (2003): 312–315.

Sadowski, J., Dłużewski, P., Kret, S., Janik, E., Łusakowska, E., Kanski, J., Presz, A., Terki, F., Charar, S., and Tang, D. 2007. Gaas: Mn nanowires grown by molecular beam epitaxy of (ga, mn) as at mnas segregation conditions. Nano Letters 7 (2007): 2724–2728.

Samia, Y. and Lutscher, F. 2012. Persistence probabilities for stream populations. Bulletin of mathematical biology 74.7 (2012): 1629–1650.

She, Z.-S., Aurell, E., and Frisch, U. 1992. The inviscid burgers equation with initial data of brownian type. Communications in mathematical physics 148.3 (1992): 623–641.

Şimşek, E. and Kim, M. 2019. Power-law tail in lag time distribution underlies bacterial persistence. Proceedings of the National Academy of Sciences 116.36 (2019): 17635–17640.

Sire, C., Majumdar, S. N., and Rüdinger, A. 2000. Analytical results for random walk persistence. Physical Review E 61.2 (2000): 1258.

Smith, A., Wiggs, J., Jonsson, H., Yan, H., Corrales, L., Nachtigall, P., and Jordan, K. 1995. Si adatom binding and diffusion on the si (100) surface: Comparison of ab initio, semiempirical and empirical potential results. The Journal of chemical physics 102 (1995): 1044–1056.

Tabe, M., Arai, K., and Nakamura, H. 1981. Effect of growth temperature on si mbe film. Japanese Journal of Applied Physics 20.4 (1981): 703.

Tamborenea, P. and Das Sarma, S. 1993. Surface-diffusion-driven kinetic growth on one-dimensional substrates. Physical Review E 48 (1993): 2575.

Williams, P. H. and Araéjo, M. B. 2000. Using probability of persistence to identify important areas for biodiversity conservation. Proceedings of the Royal Society of London. Series B: Biological Sciences 267.1456 (2000): 1959–1966.

Appendix I

NUMERICAL SIMULATION

In this dissertation, we study persistence probabilities and exponents by numerical simulation. To grow a film, we follow the MBE processes described in chapter 2, but we ignore the desorption process. A flow chart represents MBE algorithm is displayed in figure A.1. After deposition of each atom, the diffusion time τ_R of every surface atom is computed. All of the surface atoms with the lowest τ_R have a chance to diffuse. They are randomly selected to diffuse until the condition $l < l_{max}$ is violated. After that, a new atom is deposited. w is calculated from equation (2.6) at every completed layer (t). $P_{\pm}^{T,S}$ are calculated after every additional δt layers.
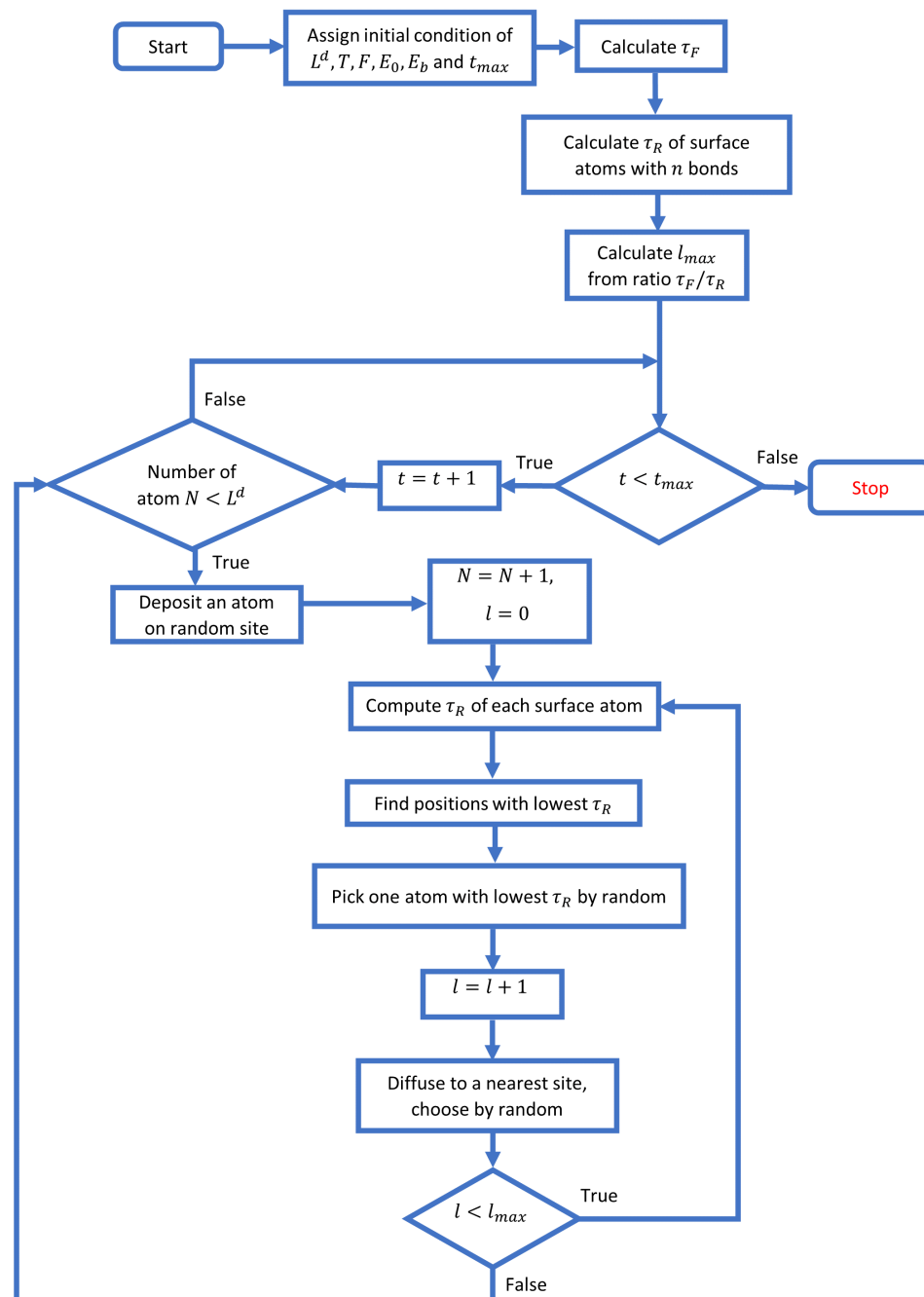
Figure A.1: Flow chart of the (2+1) MBE model simulation.

Biography

Pipitton Sanseeha was born in Kalasin, Thailand on May, 1997. He graduated from Khon Kaen University with a bachelor's degree in Physics in 2019 and then went to Chulalongkorn University for a master's degree. His field of interest includes various topics in computational physics, statistics, and machine learning.

<u>CONFERENCE PRESENTATIONS</u>

- Siam Physics Congress 2022 - Poster Presentation
  22 - 24 June 2022
  Sanseeha, P., Chanphana, R., and Chatraphorn P. Effects of Temperature on Persistence Probabilities in Molecular Beam Epitaxy Model.
  Nakhon Ratchasima, Thailand.

- The 48th International Congress on Science, Technology and Technology-based Innovation (STT48) - Poster Presentation
  29 Nov - 1 Dec 2022
  Sanseeha, P., Chanphana, R., and Chatraphorn P. Persistence Exponents of a Particular Height Fluctuation in Molecular Beam Epitaxy Model.
  Walailak University, Thailand.

<u>PROCEEDING PUBLICATION</u>

- Sanseeha, P., Chanphana, R. and Chatraphorn, P., "Persistence exponents of a particular height fluctuation in molecular beam epitaxy model", Proceedings of The 48th International Congress on Science, Technology and Technology-based Innovation (STT48), Nov 29 - Dec 1, 2022, pp. 481-486.